Chapter I.8

Transverse linear imperfections

Hannes Bartosik, Davide Gamba
CERN, Geneva, Switzerland

This chapter addresses transverse linear imperfections in particle accelerators, with a particular focus on their impact on the transverse dynamics of particle beams in circular accelerators. The primary sources of these imperfections include magnetic field errors, which arise from uncertainties in magnet strengths and calibration, as well as magnet misalignments. The theoretical framework necessary for understanding these imperfections is established, introducing concepts such as multipole expansion of magnetic fields. This foundation paves the way for addressing non-linear effects, which will be discussed in the following chapter. Practical examples, including the effects of magnetic hysteresis and quadrupole magnet misalignments, are presented to illustrate the real-world consequences of these imperfections, such as closed orbit distortion and optics function distortions like beta-beating and tune shifts, as well as coupling. Furthermore, this chapter discusses local and global closed orbit correction techniques using dipole correctors, as well as advanced methods like Singular Value Decomposition (SVD) and MICADO algorithms. The chapter also provides practical methods for estimating the impact of imperfections on closed orbit, tune shifts, beta-beating, and coupling, offering a valuable toolkit for the design and optimization of circular accelerators.

I.8.1 Introduction—sources of imperfections

In this course, we will be discussing *linear imperfections* and their impact on circular accelerators ("rings"). These imperfections, arising from magnetic field imperfections and magnet misalignment errors, affect most importantly the transverse dynamics of the particle motion. In most parts of the lecture, we will be using normalized magnet strength, i.e. magnetic field B derivatives normalized by the magnetic rigidity $B\rho = p/q$, which for a particle with charge $q = Ze$ and with total energy E (in GeV) or momentum p (in GeV/c) is given in Tm by the following relations

$$B\rho[\text{Tm}] = 3.3356\,\beta_r E[\text{GeV}]/Z, \tag{I.8.1}$$

$$= 3.3356\,p[\text{GeV/}c]/Z, \tag{I.8.2}$$

where $\beta_r = \frac{v}{c}$ is the velocity v normalized to the speed of light c, e is the elementary charge, and Z is the particle charge state which is equal to 1 for protons.

There are two main categories of imperfections that are encountered when translating an ideal lattice model into a real accelerator installation, as discussed in the following.

This chapter should be cited as: Transverse linear imperfections, H. Bartosik, D. Gamba, DOI: 10.23730/CYRSP-2024-003.341, in: Proceedings of the Joint Universities Accelerator School (JUAS): Courses and exercises, E. Métral (ed.), CERN Yellow Reports: School Proceedings, CERN-2024-003, DOI: 10.23730/CYRSP-2024-003, p. 341.

I.8.1.1 Errors in the magnet strengths

First, the physical units of the machine model defined by the accelerator physicist, i.e. the magnet strengths, must be converted into magnetic fields and eventually into currents for the power converters that feed the magnet circuits. Imperfections (i.e. errors) in the real accelerator optics can be introduced by uncertainties or errors in the magnetic field. Figure I.8.1 shows how uncertainties in the precise beam momentum, the magnet calibration and hysteresis effects, inaccuracies in the power converter regulation, and additional effects such as eddy currents introduce discrepancies between the desired magnetic field from the model and the actual magnetic field seen by the beam. An example of the magnetic hysteresis effect is shown in Fig. I.8.2. Depending on the magnetic history, e.g. if the magnet is ramped up or ramped down, the magnetic field in the magnet is different for a given excitation current.

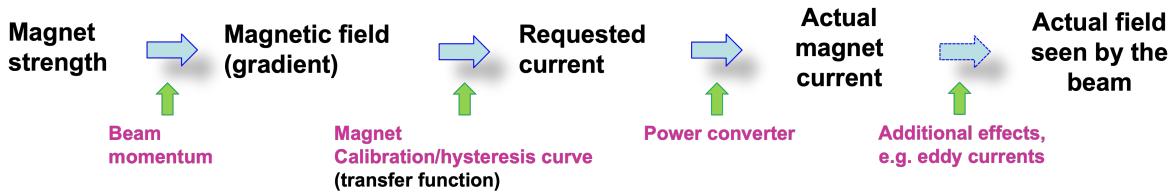

Fig. I.8.1: From magnet strength to magnetic field.

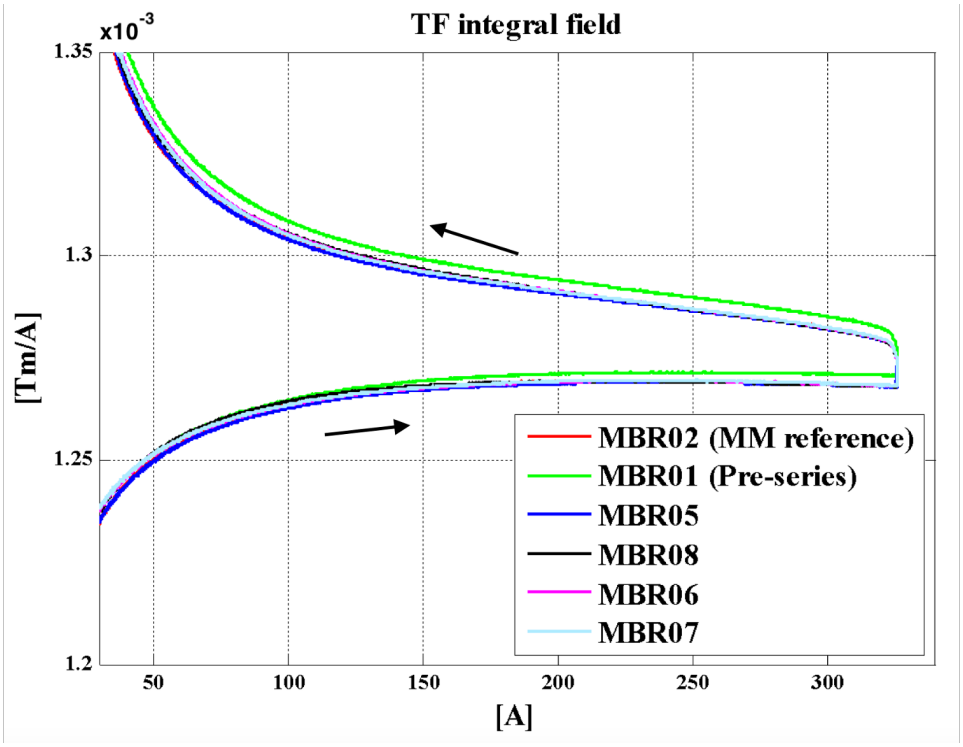

Fig. I.8.2: Example of the Extra Low ENergy Antiproton (ELENA) ring main dipoles Transfer Function (TF) of the integrated dipole field over coil excitation current along a hysteresis curve. The arrows indicate the ramping direction of the excitation current. Different colours correspond to different magnet units.

I.8.1.2 Magnet misalignments and feed-down effects

The second category of imperfections concern the alignment of accelerator magnets. Depending on the machine specific performance goals, the accelerator elements must be positioned in the accelerator tunnel within a certain accuracy. For example, the magnets of the CLIC final focusing system have to be aligned to the nanometer level. For the CERN hadron accelerators we aim for accuracies of around 0.1 mm. The alignment process implies precise measurements of the magnetic axis in the laboratory with reference to the element alignment markers used by the survey group (this process is known as fiducialization). The alignment target can be seen on the photograph of a quadrupole of the Super Proton Synchrotron (SPS) at CERN shown in Fig. I.8.3. Using these alignment targets, the survey group performs the precise in-situ alignment (positions and angles) of the element in the tunnel. Residual alignment errors are a common source of imperfections through the so-called magnetic feed-down effects.

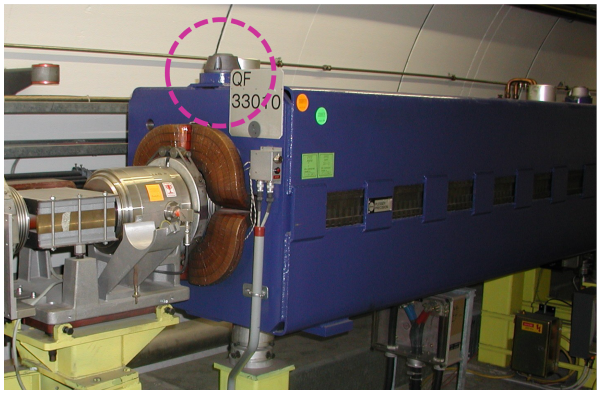

Fig. I.8.3: Alignment target (as highlighted by the purple circle) on one of the Super Proton Synchrotron (SPS) main quadrupole magnets.

To illustrate feed-down effects, let's consider a quadrupole magnet which has a horizontal misalignment of $-\delta x$, as shown in Fig. I.8.4. The magnetic field generated by this quadrupole is given by

$$\begin{aligned} B_x(\bar{x}, y) = B_x(x + \delta x, y) = G \cdot (y) \qquad &= \underbrace{Gy}_{\text{quadrupole dipole}}, \\ B_y(\bar{x}, y) = B_y(x + \delta x, y) = G \cdot (x + \delta x) &= \overbrace{Gx} + \overbrace{G\delta x}, \end{aligned} \tag{I.8.3}$$

which is equivalent to the original quadrupolar field plus a constant vertical field component corresponding to a dipolar field. Effectively, the horizontally displaced quadrupole also generates a dipole field through feed-down. This is also sketched in Fig. I.8.4.

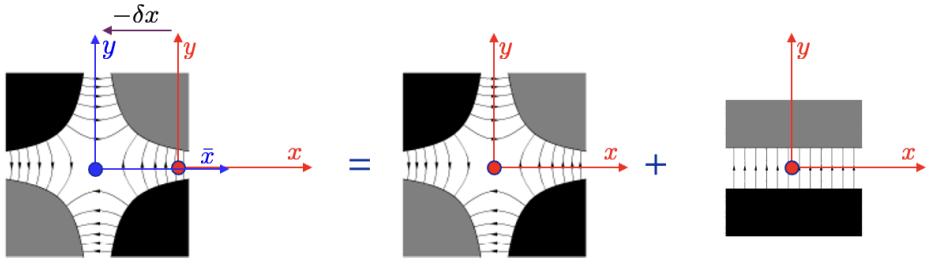

Fig. I.8.4: Feed-down effect from a horizontally displaced quadrupole.

Similarly, the magnetic field generated by a vertically displaced quadrupole as shown in Fig. I.8.5 is given by

$$\begin{aligned} B_x(x,\bar{y}) = B_x(x,y+\delta y) = G\cdot(y+\delta y) = \underbrace{Gy}_{\text{quadrupole}} + \underbrace{G\delta y}_{\text{dipole}}, \\ B_y(x,\bar{y}) = B_y(x,y+\delta y) = G\cdot(x) = \overbrace{Gx}, \end{aligned} \tag{I.8.4}$$

which is equivalent to the original quadrupolar field plus a constant horizontal field component corresponding to a *skew* dipole field. Effectively, the vertically displaced quadrupole also generates a *skew* dipole field deflecting particles in the vertical plane through the Lorentz force. We have introduced here the term *skew* dipole, which indicates that the magnetic field component is rotated compared to the normal dipolar field used for deflecting particles in the horizontal plane.

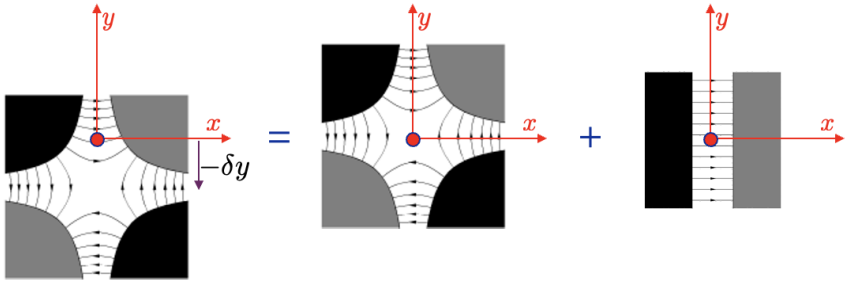

Fig. I.8.5: Feed-down effect from a vertically displaced quadrupole.

In this chapter we consider pure transverse magnetic fields, i.e. we are neglecting fringe fields. The magnetic field consists thus only of horizontal and vertical field components and we can use a multipole expansion to describe our field configuration. It is convenient to use a complex 2D representation given by

$$\mathbf{B}(x,y) = B_y(x,y) + iB_x(x,y) = \sum_{n=0}^{\infty}(B_n + iA_n)(x+iy)^n, \tag{I.8.5}$$

where the magnetic field components are given by

$$B_n = \frac{1}{n!}\frac{\partial^n B_y}{\partial x^n}\bigg|_{(0,0)} \qquad \text{and} \qquad A_n = \frac{1}{n!}\frac{\partial^n B_x}{\partial y^n}\bigg|_{(0,0)}, \tag{I.8.6}$$

where B_n represent the *normal* (also called "upright") and A_n represent the *skew* field components[1]. The *skew* field components correspond to magnetic field configurations which are rotated by an angle of $\frac{\pi}{2(n+1)}$. For example, a skew dipole ($n = 0$) corresponds to a dipole field rotated by $\frac{\pi}{2}$, i.e. a 90 degree rotated dipole field generating a vertical kick. Similarly, a skew-quadrupole ($n = 1$) field corresponds to a quadrupolar field rotated by $\frac{\pi}{4}$, and so on.

For illustration of the general behaviour of the feed-down effect, we start writing the magnetic field components B_x and B_y as the sum of all multipole components and we identify the contributions from the normal and skew components

$$\begin{aligned} B_y &= \underbrace{B_0}_{\text{dipole}} + \underbrace{B_1 x - A_1 y}_{\text{quadrupole}} + \underbrace{B_2(x^2-y^2) - 2A_2xy}_{\text{sextupole}} + \underbrace{B_3(x^3-3xy^2) - A_3(-y^3+3x^2y)}_{\text{octupole}} + \ldots, \\ B_x &= \overbrace{A_0} + \overbrace{A_1 x + B_1 y} + \overbrace{A_2(x^2-y^2) + 2B_2xy} + \overbrace{A_3(x^3-3xy^2) + B_3(-y^3+3x^2y)} + \ldots, \end{aligned} \tag{I.8.9}$$

For investigating the effect of a pure horizontal displacement $\bar{x} = x + \delta x$, we analyze the magnetic field components along the horizontal axis, i.e. for $y = 0$. Starting from Eq. I.8.9, we find that a horizontally displaced multipole field of order n, i.e. a "$2(n+1)$ pole"

$$\begin{aligned} &B_x(y{=}0) = 0, \\ &B_y(y{=}0) = \underbrace{B_n\bar{x}^n}_{2(n+1)\text{-pole}} = B_n(x+\delta x)^n = B_n\Big(\underbrace{x^n}_{2(n+1)\text{-pole}} + \underbrace{n\delta x x^{n-1}}_{2n\text{-pole}} + \underbrace{\tfrac{n(n-1)}{2}\delta x^2 x^{n-2}}_{2(n-1)\text{-pole}} + \ldots + \underbrace{(\delta x)^n}_{\text{dipole}}\Big), \\ &B_x(y{=}0) = \overbrace{A_n\bar{x}^n} = A_n(x+\delta x)^n = A_n\Big(\overbrace{x^n} + \overbrace{n\delta x x^{n-1}} + \overbrace{\tfrac{n(n-1)}{2}\delta x^2 x^{n-2}} + \ldots + \overbrace{(\delta x)^n}\Big), \\ &B_y(y{=}0) = 0, \end{aligned} \tag{I.8.10}$$

results in a series of lower order normal multipole components from a $2n$ pole all the way down to the dipole components. In particular, a *horizontally displaced normal* multipole of strength B_n (upper two lines of Eq. I.8.10) creates *normal* feed-down components. Conversely, a *horizontally displaced skew* multipole of strength A_n (lower two lines of Eq. I.8.10) creates *skew* feed-down components. It should also be mentioned that the decreasing order of feed-down multipole components have a strength that is proportional to the initial magnet strength and more importantly proportional to an increasing power of the misalignment δx. Since this offset is usually small, the feed-down multipole components become less important for lower orders. It should also be noted that we have considered here the components along the horizontal axis only. However, the reader than verify that the obtained expressions of the feed-down

[1] In some occasions it is useful to consider the magnetic field expansion in normalized multipole strengths as follows

$$\mathbf{B} = B_y + iB_x = B\rho\sum_{n=0}^{\infty}(k_n + ij_n)\frac{(x+iy)^n}{n!}, \tag{I.8.7}$$

where the normalized magnet field components are given by

$$k_n = \frac{1}{B\rho}\frac{\partial^n B_y}{\partial x^n}\bigg|_{(0,0)} = \frac{n!}{B\rho}B_n\bigg|_{(0,0)} \quad \text{and} \quad j_n = \frac{1}{B\rho}\frac{\partial^n B_x}{\partial y^n}\bigg|_{(0,0)} = \frac{n!}{B\rho}A_n\bigg|_{(0,0)}. \tag{I.8.8}$$

components also hold for $y \neq 0$.

Performing a similar analysis for vertical misalignments we investigate the magnetic field components along the vertical axis, i.e. for $x = 0$. We find that

$$\text{for } n \text{ even} \begin{cases} B_y(x=0) = i^n B_n \bar{y}^n \\ \\ B_x(x=0) = i^n A_n \bar{y}^n \end{cases}, \qquad \text{for } n \text{ odd} \begin{cases} B_y(x=0) = i^{n+1} A_n \bar{y}^n \\ \\ B_x(x=0) = i^{n-1} B_n \bar{y}^n \end{cases}, \tag{I.8.11}$$

which means that a vertical offset in *normal(skew)* magnets of order n results in *alternating skew(normal) and normal(skew)* feed-down components of all lower orders. To illustrate this, we consider as example a normal multipole with n even, and write the vertical field component at $x = 0$ explicitly for a vertical offset δy, which yields

$$B_y(x{=}0) = i^n B_n (y + \delta y)^n = \; i^n B_n (y^n + n\delta y y^{n-1} + \tfrac{n(n-1)}{2} \delta y^2 y^{n-2} + \cdots + (\delta y)^n). \tag{I.8.12}$$

Comparing with Eq. I.8.9, we find indeed that this vertically shifted normal multipole of order n will create skew feed-down components of order $n-1, n-3, \ldots$ and normal feed-down components of order $n-2, n-4, \ldots$ all the way down to the dipole component.

I.8.1.2.1 Problem 1

a) Derive an expression for the resulting magnetic field components (B_x and B_y) when the closed orbit in a normal sextupole is horizontally displaced by $-\delta x$ from its reference position.

Hint: the field generated by a sextupole is

$$B_y(x, y) = B_2(x^2 - y^2), \tag{I.8.13}$$
$$B_x(x, y) = B_2(2xy). \tag{I.8.14}$$

a) Do the same for an octupole.

Hint: the field generated by an octupole is

$$B_y(x, y) = B_3(+x^3 - 3xy^2), \tag{I.8.15}$$
$$B_x(x, y) = B_3(-y^3 + 3x^2 y). \tag{I.8.16}$$

I.8.1.2.2 Solution to problem 1

a) We can use the following substitution:

$$x \to \bar{x} = x - (-\delta x) = x + \delta x$$

For a horizontally displaced sextupole one obtains:

$$B_y(x+\delta x, y) = B_2\left((x+\delta x)^2 - y^2\right) = B_2x^2 + 2B_2x\delta x + B_2(\delta x)^2 - B_2y^2 \quad \text{(I.8.17)}$$

$$= \underbrace{B_2(x^2-y^2)}_{\text{sextupole}} + \underbrace{2B_2(\delta x)x}_{\text{quadrupole}} + \underbrace{B_2(\delta x)^2}_{\text{dipole}} \quad \text{(I.8.18)}$$

$$\text{(I.8.19)}$$

$$B_x(x+\delta x, y) = \overbrace{B_2(2xy)} + \overbrace{2B_2(\delta x)y} \quad \text{(I.8.20)}$$

b) Similarly, for a horizontally displaced closed orbit in an octupole

$$B_y(x+\delta x, y) = B_3\left((x+\delta x)^3 + 2(\delta x)x^2 + 3(\delta x)^2x + (\delta x)^3 - 3xy^2 - 3(\delta x)y^2\right) \quad \text{(I.8.21)}$$

$$= B_3(x^3 - 3xy^2) + 3B_3(\delta x)(x^2-y^2) + 3B_3(\delta x)^2x + B_3(\delta x)^3 \quad \text{(I.8.22)}$$

$$B_x(x+\delta x, y) = B_3\left(-y^3 + 3(x^2 + 2(\delta x)x + (\delta x)^2)y\right) \quad \text{(I.8.23)}$$

$$= B_3(-y^3 + 3x^2y) + 3B_3(\delta x)2xy + 3B_3(\delta x)^2y \quad \text{(I.8.24)}$$

And from direct comparison

$$B_y(x+\delta x, y) = \underbrace{B_3(x^3-3xy^2)}_{\text{octupole}} + \underbrace{3B_3(\delta x)(x^2-y^2)}_{\text{sextupole}} + \underbrace{3B_3(\delta x)x}_{\text{quadrupole}} + \underbrace{B_3(\delta x)^3}_{\text{dipole}} \quad \text{(I.8.25)}$$

$$\text{(I.8.26)}$$

$$B_x(x+\delta x, y) = \overbrace{B_3(-y^3+3x^2y)} + \overbrace{3B_3(\delta x)2xy} + \overbrace{3B_3(\delta x)^2y} \quad \text{(I.8.27)}$$

I.8.1.2.3 Problem 2

ELENA is a small ring (30.4 m circumference) that receives anti-protons with a kinetic energy of 5.3 MeV from the Antiproton Decelerator (AD). The ring is composed of 25 cm-long quadrupoles.

a) Compute the normalized strength of the quadrupoles assuming a gradient of 1.4 T/m.

b) What is the trajectory kick, in radians, that an anti-proton receives when entering in a focusing quadrupole with a 1 mm positive offset with respect to the quadrupole magnetic axis in the focusing plane (x)?

c) What is the direction of the kick (positive/negative x/y)?

I.8.1.2.4 Solution to problem 2

a) – The magnetic rigidity is

$$B\rho\,[\text{Tm}] = 3.3356\,\beta_r E\,[\text{GeV}].$$

– We need to compute the total energy which is

$$E = T + E_0 = 0.0053 + 0.9383 = 0.9436\,\text{GeV}.$$

– Now we need to compute the relativistic beta. First, we compute the relativistic gamma

$$\gamma_r = \frac{E}{E_0} = \frac{0.9436}{0.9383} = 1.0056,$$

and the relativistic beta is

$$\beta_r = \sqrt{1 - 1/\gamma_r^2} = 0.1058.$$

– The magnetic rigidity is then

$$B\rho = 3.3356\,\beta_r E = 0.3331\,\text{Tm}.$$

– The normalised strength, for a gradient of 1.4 T/m, is

$$k_1 = \frac{1!}{B\rho} B_1 = \frac{1.4}{0.3331} = 4.203\,\frac{1}{\text{m}^2}.$$

– The **integrated** normalised strength of the quads is

$$k_1 L = 4.203 \cdot 0.25 = 1.050\,\frac{1}{\text{m}}.$$

b) For a particle entering with an offset of 0.001 m, the kick is

$$k_1 L x = 1.050 \cdot 0.001 = 1.050\,\text{mrad}.$$

c) Since it is a **focusing quadrupole**, and the particle enters with a **positive** x **offset**, then the kick is **toward negative** x **values**.

I.8.2 Closed-orbit distortion

I.8.2.1 Illustration of closed-orbit distortion

A circular accelerator (like a synchrotron) lattice is usually composed of a repetition of basic 'cells'. A simple FODO (Focusing-Drift-Defocusing-Drift) cell typically contains dipole magnets to guide (or bend) the beam around the machine, quadrupole magnets to focus the beam, beam position monitors (BPMs) to measure the transverse beam position, small dipole corrector magnets for beam steering and possibly also sextupole magnets to control the off-energy focusing (i.e. the chromaticity). A sketch of a typical FODO cell is shown in Fig. I.8.6.

To illustrate the impact of an imperfection resulting in a closed-orbit distortion, we start from a toy model representing a machine built from a basic FODO lattice as shown in Fig. I.8.7. In this figure, each vertical bar at the top corresponds to a horizontally focusing (bar pointing upwards) or a horizontally

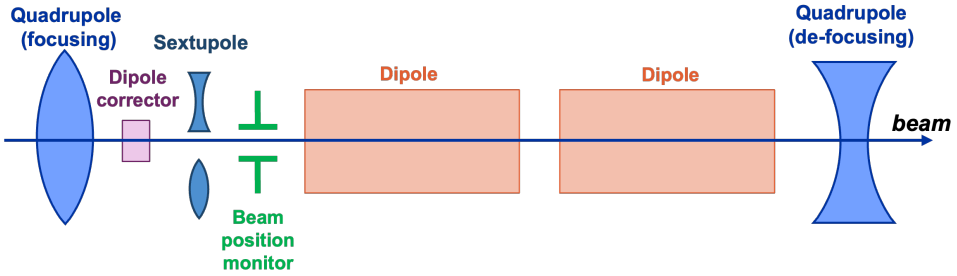

Fig. I.8.6: Sketch of a typical FODO cell (not to scale).

defocusing (bar pointing downwards) quadrupole. Our toy machine consists of 16 FODO cells. As this case shows the ideal machine without any imperfection, launching a particle with an offset of around 4 mm in the horizontal position results in betatron oscillations around the design orbit, i.e. around $x = 0$ along the machine. As shown in the figure, after 100 turns the particle trajectories trace out a nice beam envelope along the machine. On the right-hand side we show the particle phase space at the end of the machine, i.e. at $s = C$ (where C denotes the machine circumference). Indeed the phase-space ellipse is centered around the origin, i.e. around $x = 0$ and $x' = 0$ as indicated by the green dot.

Let's now investigate what happens if the FODO lattice contains an imperfection in the form of a dipole error resulting in a deflection θ. To illustrate this, we take the simple FODO lattice example from before and start tracking a particle with initial conditions $x, x' = 0$. Figure I.8.8 (top) shows the resulting particle trajectory for the first turn. Note how the dipole error, indicated by the little purple box in the lattice schematic, gives a kick to the particle and thus excites a betatron oscillation. Continuing the tracking until reaching 100 turns as shown in Fig. I.8.8 (bottom), we observe how the particle oscillates around a distorted closed orbit as indicated by the thick red line. The closed orbit corresponds to the evolution of the center of the phase-space ellipse along the machine circumference. For illustration, the phase-space ellipse at the end of the machine is also shown and it is clear how its center is shifted.

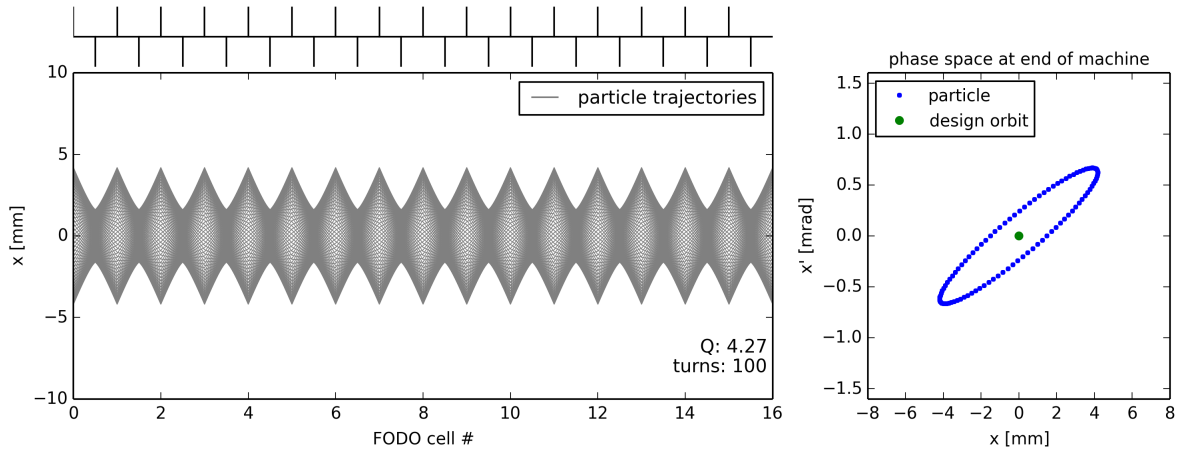

Fig. I.8.7: Particle trajectories in a FODO lattice - no errors.

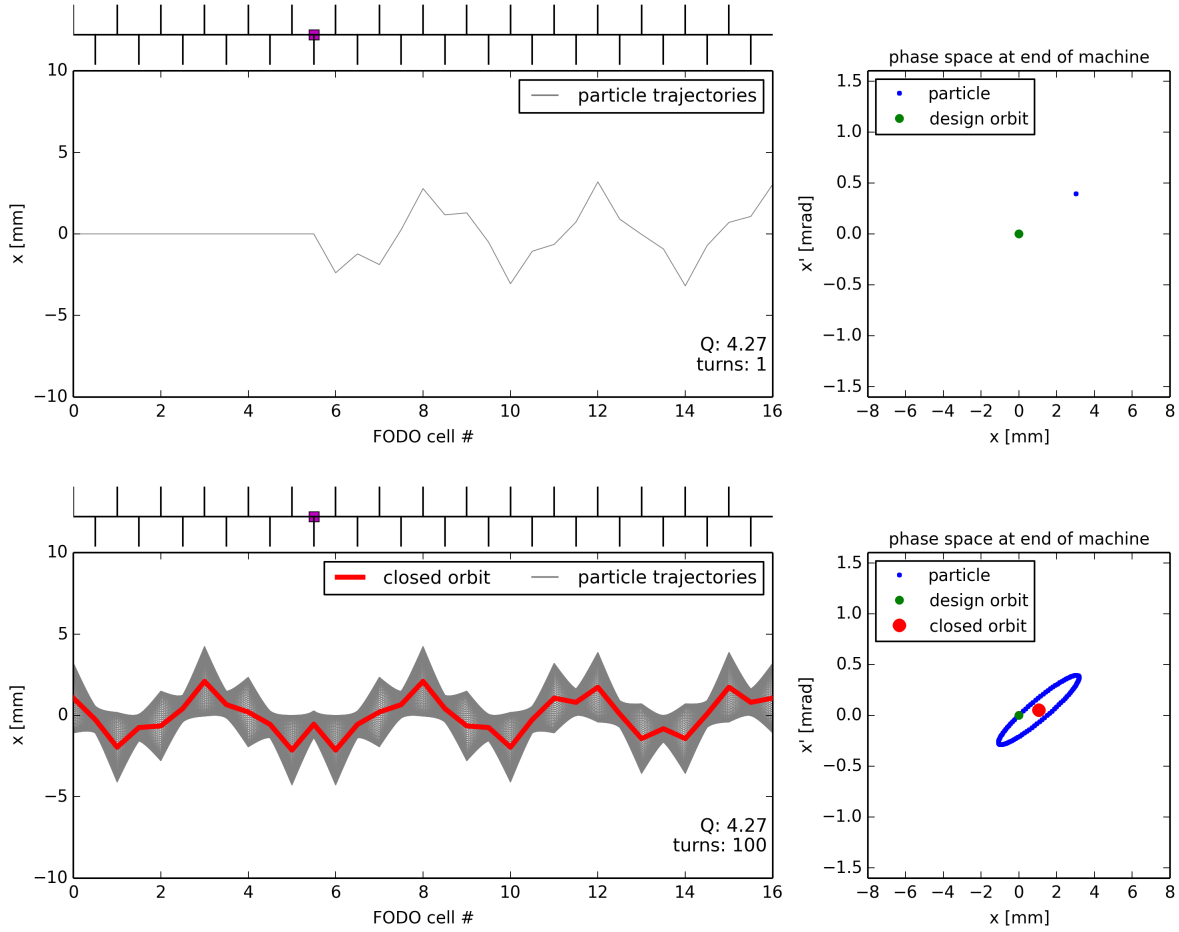

Fig. I.8.8: Particle trajectories in a FODO lattice - single-dipole error, result after 1 turn (top) and after 100 turns (bottom).

I.8.2.2 Closed orbit from a single-dipole kick

In the following, we will calculate the closed-orbit distortion resulting from a single-dipole error. Consider a single-dipole kick $\theta = \delta u'_0 = \delta u'(s_0) = \frac{\delta(Bl)}{B\rho}$ (thin-lens approximation) at $s = s_0$ as shown in Fig. I.8.9 (top). Note that we use here u as the transverse coordinate, which represents either the horizontal position x or the vertical position y.

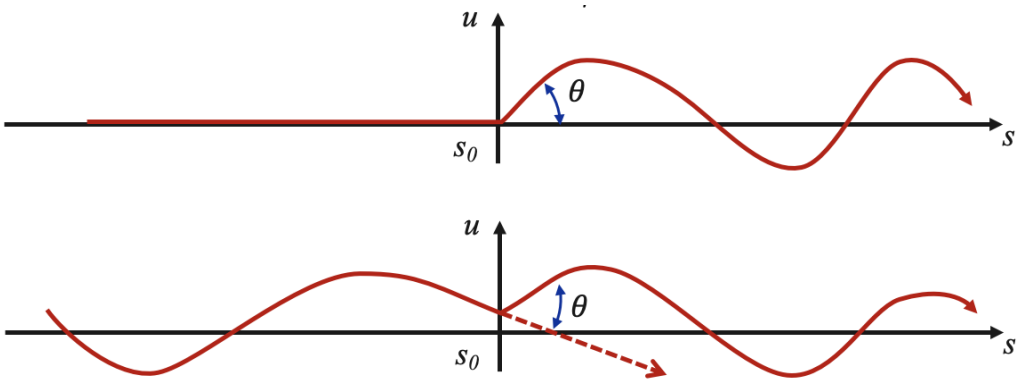

Fig. I.8.9: Change of trajectory from a single-dipole kick (top) and closed orbit resulting from a single-dipole kick (bottom).

The coordinates of a single particle at a downstream location s can be computed using the transport matrix $M_{s_0,s}$ from location s_0 to location s expressed as a function of the Twiss lattice parameters (see Chapter I.3 on transverse beam dynamics)

$$\begin{pmatrix} u_s \\ u'_s \end{pmatrix} = M_{s_0,s} \begin{pmatrix} 0 \\ \theta \end{pmatrix}, \tag{I.8.28}$$

where

$$M_{s_0,s} = \begin{bmatrix} \sqrt{\frac{\beta_s}{\beta_{s_0}}}(\cos\psi_{s_0,s} + \alpha_{s_0}\sin\psi_{s_0,s}) & \sqrt{\beta_s\beta_{s_0}}\sin\psi_{s_0,s} \\ \frac{\alpha_{s_0}-\alpha_s}{\sqrt{\beta_s\beta_{s_0}}}\cos\psi_{s_0,s} - \frac{1+\alpha_s\alpha_{s_0}}{\sqrt{\beta_s\beta_{s_0}}}\sin\psi_{s_0,s} & \sqrt{\frac{\beta_{s_0}}{\beta_s}}(\cos\psi_{s_0,s} - \alpha_s\sin\psi_{s_0,s}) \end{bmatrix}. \tag{I.8.29}$$

Since we want the orbit to be closed on itself after one turn, (see Fig. I.8.9 (bottom)), we have to solve the following equation

$$\begin{bmatrix} \cos(2\pi Q) + \alpha_0\sin(2\pi Q) & \beta_0\sin(2\pi Q) \\ -\frac{1+\alpha_0^2}{\beta_0}\sin(2\pi Q) & \cos(2\pi Q) - \alpha_0\sin(2\pi Q) \end{bmatrix} \begin{pmatrix} u_0 \\ u'_0 \end{pmatrix} + \begin{pmatrix} 0 \\ \theta \end{pmatrix} = \begin{pmatrix} u_0 \\ u'_0 \end{pmatrix}, \tag{I.8.30}$$

which only depends on the Twiss functions at the s_0 location and the machine tune Q. The initial conditions of the closed orbit at the location of the kick are obtained as

$$u_0 = \frac{\theta}{2}\frac{\beta_0}{\tan(\pi Q)} \qquad \text{and} \qquad u'_0 = \frac{\theta}{2}\left(1 - \frac{\alpha_0}{\tan(\pi Q)}\right). \tag{I.8.31}$$

For any location s around the ring, the closed-orbit distortion Δu generated by a kick θ in s_0 is obtained

as

$$\Delta u_s = \underbrace{\theta_{s_0} \frac{\sqrt{\beta_s \beta_{s_0}}}{2\sin(\pi Q)}}_{\text{maximum orbit distortion amplitude}} \cos(\pi Q - |\psi_s - \psi_{s_0}|), \tag{I.8.32}$$

where β_s denotes the beta function at location s and β_{s_0} the beta function at location s_0, and ψ_s, ψ_{s_0} are the phase advances at locations s and s_0. Note that this expression consists of the oscillatory term $\cos(\pi Q - |\psi_s - \psi_{s_0}|)$ and the term $\theta_{s_0} \frac{\sqrt{\beta_s \beta_{s_0}}}{2\sin(\pi Q)}$ that defines the maximum closed-orbit distortion amplitude around the machine. We highlight that the impact of a localised dipole error results in a closed-orbit distortion proportional to $\sqrt{\beta_{s_0}}$, i.e. the impact is higher for errors located in a region with a large beta function. Furthermore, we observe that the maximum closed-orbit distortion amplitude has a strong dependence on the tune due to the denominator $\sin(\pi Q)$.

I.8.2.3 Dependence of closed-orbit distortion amplitude on the tune-integer resonance

The impact of a single-dipole error on the closed orbit depends strongly on the tune of the machine (see Eq. I.8.32) as illustrated in Fig. I.8.10. While the same dipole error results in a modest closed-orbit distortion at a tune of $Q = 4.47$, the impact is about 5 times higher at $Q = 4.07$ and about 20 times higher at $Q = 4.02$. In fact the closed-orbit distortion is most critical for tunes close to integer values, for which the closed orbit becomes unstable due to the expression $2\sin(\pi Q)$ in the denominator going to zero. Conversely, for a tune close to half-integer values the same term attains its maximum value of ± 2. In other words, the closed-orbit distortion is minimum. This behaviour can also be illustrated in phase space as shown in Fig. I.8.11. For integer tunes (left picture), particles return to the same position (y in this illustration) turn after turn and a dipole error adds up and systematically increases the oscillation amplitude. As this happens for all particles in the same way, the closed orbit is unstable. For half-integer tunes (right picture), the kick from the dipole error cancels out every other turn and the particle oscillation amplitude remains bounded. It is due to this cancellation that the impact on the closed-orbit distortion is minimum for half-integer tunes. In other words, integer tunes have to be avoided in the presence of dipole errors due to the integer resonance, while half-integer tunes are not harmful in this case.

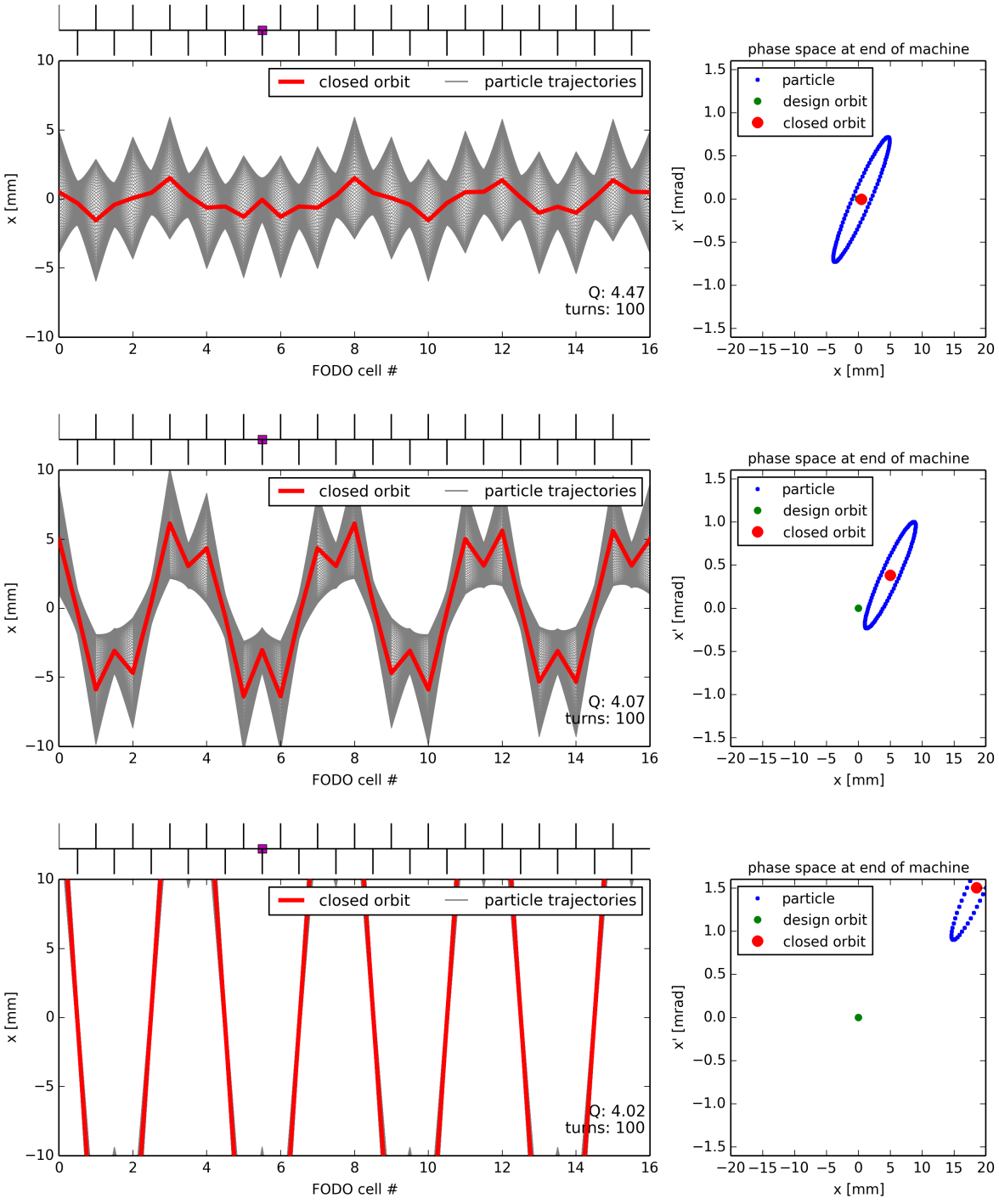

Fig. I.8.10: Impact of a single-dipole error on the closed orbit for different tunes: $Q = 4.47$ (top), $Q = 4.07$ (middle) and $Q = 4.02$ (bottom). The strength of the dipole error is the same for all three cases.

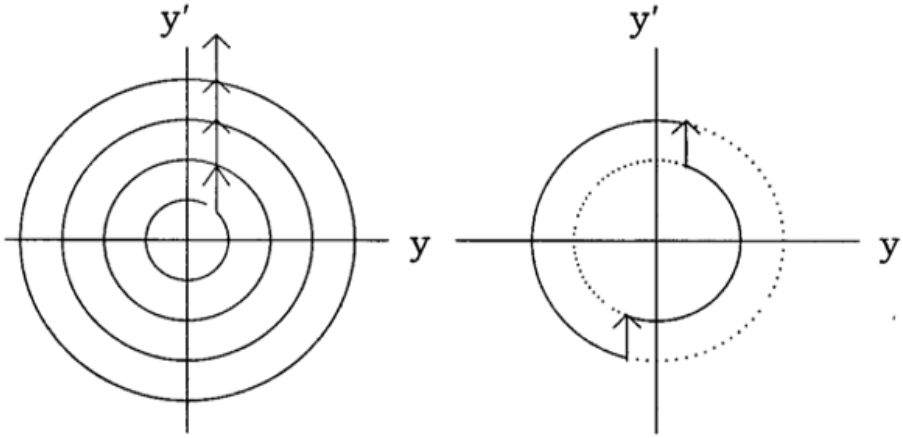

Fig. I.8.11: Effect of a dipole error at integer (left) and half-integer (right) tunes.

I.8.2.4 Localizing closed-orbit errors

Figure I.8.12 shows schematically how a single-dipole error affects the closed orbit for different tunes ranging from 6.1 to 6.9. Note that for tunes close to the integer resonance, the overall closed-orbit distortion is large, while for tunes further away from the integer values the impact becomes smaller, as expected from Eq. I.8.32. Depending on the tune, the closed orbit exhibits a bit more than six or almost seven complete oscillations. The location of the dipole error can be identified by the "kink" in the closed-orbit oscillation, as also indicated by the red arrow in the schematic. This kink can also be used to identify a single-dipole error in a beam orbit measurement. To illustrate this we take a look at an example orbit measurement of the Large Hadron Collider (LHC). Figure I.8.13 shows a measurement of the horizontal closed orbit along the LHC circumference. In this case there is only a single-dipole kick, as the measurement is taken with respect to a reference closed orbit. Each vertical green bar corresponds to the measurement of one LHC BPM. However, in this representation it is not easy to identify the location of the dipole kick. Only when taking the same data and plotting the beam position normalized by the square root of the corresponding local beta function ($x/\sqrt{\beta}$) as a function of the betatron phase

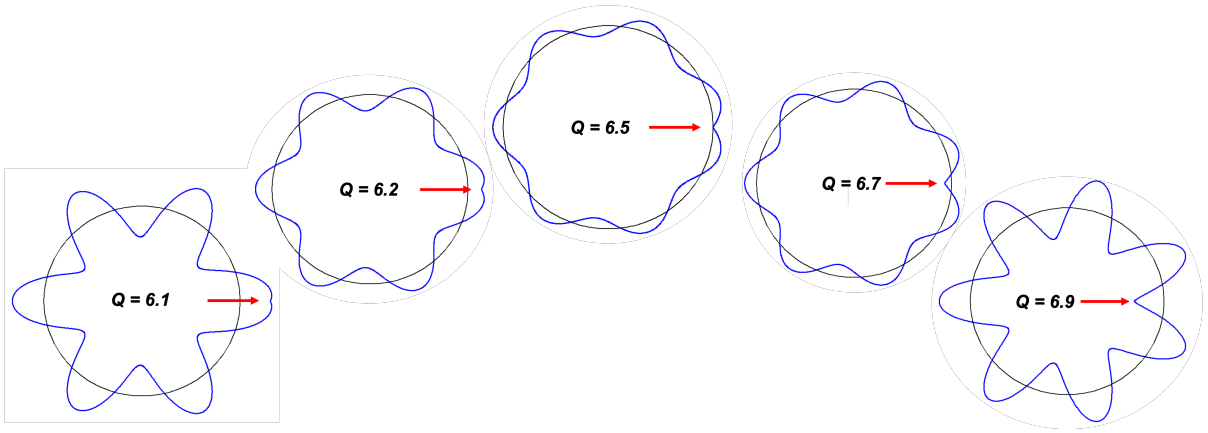

Fig. I.8.12: Schematic representation of closed-orbit distortions for different tunes.

advance ψ, the kink can be identified clearly. This approach can be quite handy in routine operation when searching for a single localized dipole kick, e.g. identifying the failure of single-dipole correctors, missing strength of individual main dipoles due to inter-turn shorts, remnent field of strong bumper magnets used for beam extraction, and other similar situations.

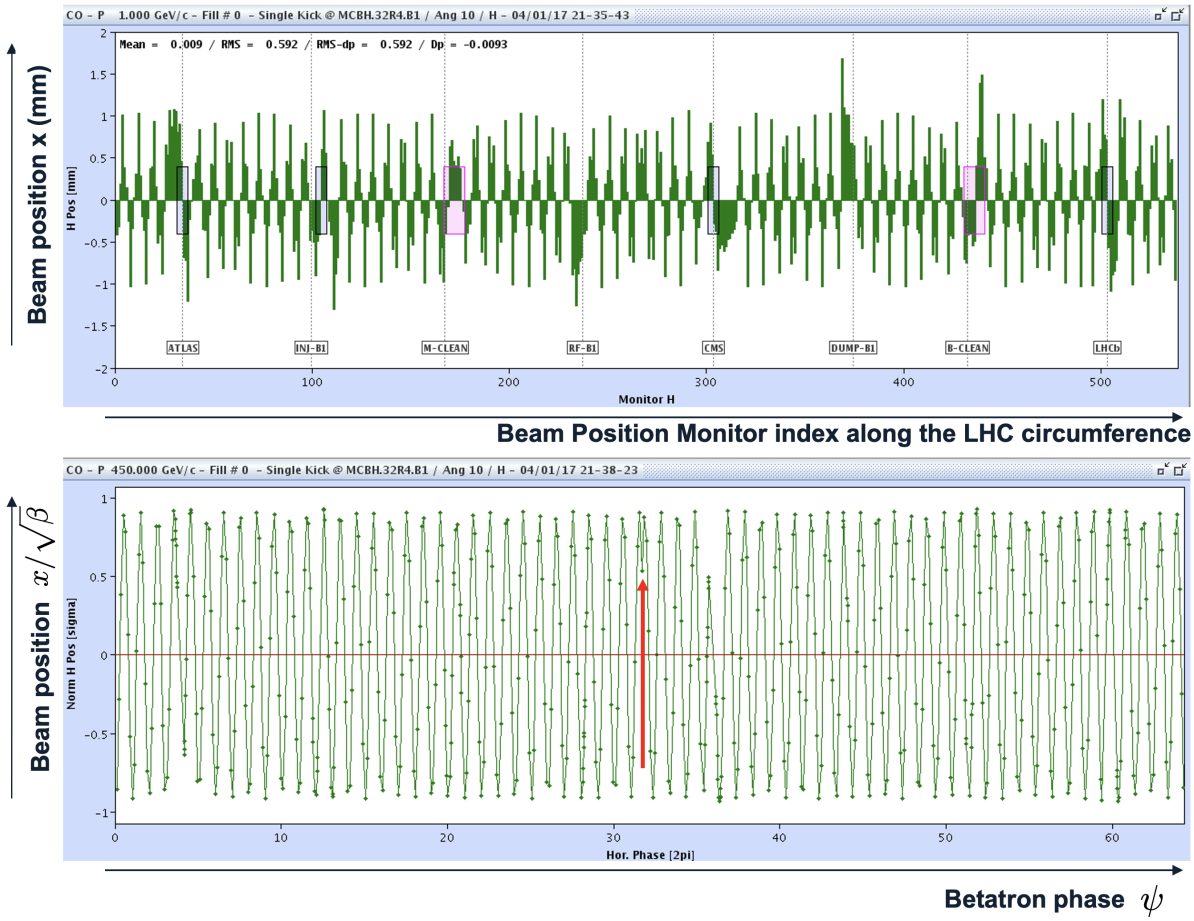

Fig. I.8.13: Measurement of the horizontal closed orbit in the LHC. The data corresponds to the difference orbit, where only a single-dipole error deflection was added with respect to a reference closed orbit. The raw BPM measurement is shown on the top, while the normalized closed-orbit oscillation as a function of the phase advance is shown on the bottom. The location of the dipole deflection is indicated by the red arrow.

I.8.2.5 Global closed-orbit distortion

In a realistic accelerator, dipole kicks resulting in closed-orbit distortion can be generated by various sources, typically related to the presence of a constant transverse magnetic field error (δB_u) at some location (s). In general, the angular kick ($d\theta$) received by the beam is

$$d\theta = \frac{\delta B_u(s) ds}{B\rho}. \tag{I.8.33}$$

For the most common sources, the integrated deflection θ_j produced by the j^{th} error can be expressed as

– Integrated dipole field error

$$\theta_j = \frac{\delta(B_j l_j)}{B\rho}, \tag{I.8.34}$$

where $B_j l_j$ is the integrated dipole field.

– Dipole roll

$$\theta_j = \frac{B_j l_j \sin\phi_j}{B\rho}, \tag{I.8.35}$$

where ϕ_j is the roll angle of the dipole around its longitudinal axis.

– Quadrupole displacement

$$\theta_j = \frac{G_j l_j \delta u_j}{B\rho}, \tag{I.8.36}$$

where δu_j is the transverse displacement of the quadrupole, G_j is the quadrupole gradient and l_j is the length of the quadrupole.

The formalism for treating the general case of closed-orbit distortion was first introduced by Courant and Snyder in 1957 [1]. As we consider linear betatron motion only, the total orbit distortion at a general location s can be expressed as the integral of all perturbations encountered along the ring

$$u(s) = \frac{\sqrt{\beta(s)}}{2\sin(\pi Q)} \int_s^{s+C} \frac{\delta B_u(\tau)}{B\rho} \theta(\tau) \sqrt{\beta(\tau)} \cos\left(\pi Q - |\psi(s) - \psi(\tau)|\right) d\tau. \tag{I.8.37}$$

Approximating the errors as delta functions at n locations, the distortion at the i^{th} observation point (e.g. at a BPM) is obtained as

$$u_i = \frac{\sqrt{\beta_i}}{2\sin(\pi Q)} \sum_{j=i+1}^{i+n} \theta_j \sqrt{\beta_j} \cos\left(\pi Q - |\psi_i - \psi_j|\right), \tag{I.8.38}$$

with j indicating each single kick produced by the n errors.

During the design stage of a circular accelerator, it is interesting to estimate the expected closed-orbit distortion induced by a random distribution of errors in n magnets. Such calculations are typically done to specify tolerances of magnet alignments and field errors of the linear magnets (dipoles and quadrupoles). By squaring the orbit distortion expression and averaging over the angles (considering uncorrelated errors), the expectation (rms) value of the closed-orbit distortion is obtained as

$$u_{\text{rms}}(s) = \frac{\sqrt{\beta(s)}}{2\sqrt{2}|\sin(\pi Q)|} \left(\sum_j \sqrt{\beta_j} \theta_j \right)_{\text{rms}} = \frac{\sqrt{n\beta(s)\beta_{\text{rms}}}}{2\sqrt{2}|\sin(\pi Q)|} \theta_{\text{rms}}. \tag{I.8.39}$$

To illustrate this we look at the example of the Spallation Neutron Source (SNS) ring: with its 32 dipoles ($\beta = 6$ m) and 54 quadrupoles ($\beta = 30$ m), and a tune of $Q = 6.2$, and assuming 1 mrad rms kicks either at dipoles or at quadrupoles, one obtains:

– The rms orbit distortion in the dipoles

$$u_{\text{rms}}^{\text{dip}} = \frac{\sqrt{6 \cdot 6 \cdot 32}}{2\sqrt{2}|\sin(6.2\pi)|} \cdot 10^{-3} \approx 2\,\text{cm}.$$

– In the quadrupoles, for equivalent kicks

$$u_{\text{rms}}^{\text{quad}} = \frac{\sqrt{30 \cdot 30 \cdot 54}}{2\sqrt{2}|\sin(6.2\pi)|} \cdot 10^{-3} \approx 13\,\text{cm}.$$

I.8.2.5.1 Problem 3

The SNS proton ring with kinetic energy of 1 GeV and a circumference of 248 m has 18, 1 m-long focusing quadrupoles, each with a gradient of 5 T/m. In one of the quadrupoles, the horizontal and vertical β functions are $12\,\text{m}$ and $2\,\text{m}$, respectively. The rms β function in both planes on the focusing quadrupoles is 8 m.

a) With a horizontal tune of 6.23 and a vertical tune of 6.2, compute the expected horizontal and vertical orbit distortions on a single focusing quadrupole induced by horizontal and vertical misalignments of 1 mm rms in all the quadrupoles.

b) What happens to the horizontal and vertical closed-orbit distortions if the horizontal tune drops to 6.1, and 6.01?

I.8.2.5.2 Solution to problem 3

a) – The rms orbit distortion is given by

$$u_{\text{rms}}(s) = \frac{\sqrt{N\beta(s)\beta_{\text{rms}}}}{2\sqrt{2}|\sin(\pi Q)|}\theta_{\text{rms}}.$$

– We need to determine the rms kick angle, which for a quadrupole displacement is given by

$$\theta_{\text{rms}} = \frac{GL}{B\rho}(\delta u)_{\text{rms}}.$$

– For computing the magnetic rigidity $B\rho$ we need the total energy, which is

$$E = T + E_0 = 1.938\,\text{GeV}.$$

– W compute the relativistic beta from the relativistic gamma

$$\gamma_r = \frac{E}{E_0} = 2.07 \;\Rightarrow\; \beta_r = \sqrt{1 - 1/\gamma_r^2} = 0.875.$$

– The magnetic rigidity is then

$$B\rho = 3.3356\,\beta_r E\,[\text{GeV}] = 5.657\,\text{Tm},$$

and the rms angle in both planes is

$$\theta_{\text{rms}} = 8.8 \times 10^{-4}\,\text{rad}.$$

– Now we can calculate the rms orbit distortion on the single focusing quad

$$x_{\text{rms}}(s) = \frac{\sqrt{N\beta_x(s)}\beta_{\text{rms}}}{2\sqrt{2}|\sin(\pi Q_x)|}\theta_{\text{rms}} = \frac{\sqrt{18\times 12\times 8}}{2\sqrt{2}|\sin(6.23\pi)|}\times 8.8\times 10^{-4} = 19.6\,\text{mm}.$$

– The vertical is

$$y_{\text{rms}}(s) = \frac{\sqrt{N\beta_y(s)}\beta_{\text{rms}}}{2\sqrt{2}|\sin(\pi Q_y)|}\theta_{\text{rms}} = \frac{\sqrt{18\times 2\times 8}}{2\sqrt{2}|\sin(6.20\pi)|}\times 8.8\times 10^{-4} = 9\,\text{mm}.$$

b) – For $Q_x = 6.1$ the horizontal orbit distortion becomes

$$x_{\text{rms}}(s) = 41.9\,\text{mm}.$$

– For $Q_x = 6.01$ we have

$$x_{\text{rms}}(s) = 0.41\,\text{m}.$$

– For both cases, the vertical rms orbit distortion remains unchanged.

I.8.2.6 Closed-orbit correction

In particle accelerators, maintaining the precise alignment and trajectory of the particle beams is critical for optimal performance. Various imperfections can lead to closed-orbit distortions as mentioned above, which need to be corrected, e.g. to minimize particle loss on the vacuum chambers. Generally speaking, one needs to develop methods to measure the beam orbit using BPMs and to minimize the closed-orbit distortion by deploying closed-orbit dipole corrector magnets. The closed orbit can be corrected locally, correcting directly at the source of the error, e.g. by introducing closed-orbit bumps. For the global closed-orbit correction, various methods have been developed, such as a harmonic correction by minimizing components of the closed-orbit frequency response from Fourier analysis; the MICADO algorithm that searches for the most efficient corrector for minimizing the rms orbit; or a least square minimization using the orbit response matrix of dipole correctors using SVD.

From the previous analysis above we have observed that the impact of a kick on the closed orbit is proportional to $\sqrt{\beta}$ at the location of the kick, and to $\sqrt{\beta}$ at the location of observation. It is thus advantageous to install closed-orbit correctors at locations with large β functions, and also BPMs at locations with large β functions. The choice of the machine layout can thus already help in optimising the closed-orbit correctability of a machine by placing horizontal or vertical dipole correctors and BPMs close to focusing or defocusing quadrupoles, respectively. An example is the FODO lattice of the SPS

ring shown in Fig. I.8.14, in which horizontal BPMs and horizontal orbit correctors were installed next to focusing quadrupoles, and conversely vertical BPMs and vertical orbit correctors were installed next to defocusing quadrupoles.

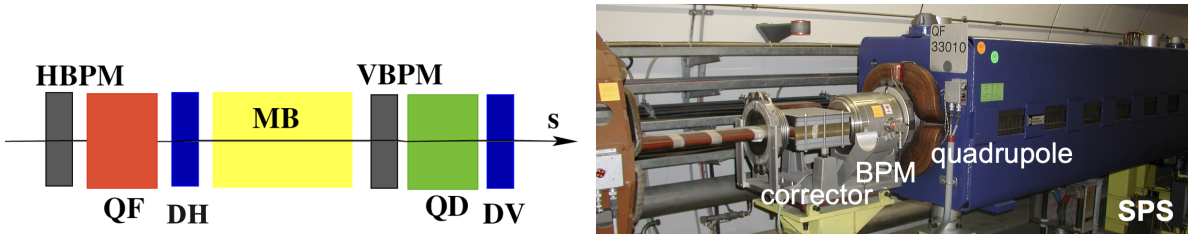

Fig. I.8.14: Example diagram (left) and actual disposition in the SPS (right) of dipole correctors and BPMs close to quadrupoles.

For machines with less regular optics, special attention is required for the locations where beta-functions reach maxima (e.g. insertion regions in a collider) and/or where the phase advance is quickly evolving.

I.8.2.7 Closed-orbit correction - local

Often it is needed to steer the closed orbit away from the nominal trajectory in a localized part of a circular accelerator. Typical examples are local orbit correction (or steering around local aperture restrictions) using a few correctors, e.g. Fig. I.8.15, or bumps required for injection / extraction, e.g. Fig. I.8.16. Standard "bump" configurations exist, using a limited number of correctors.

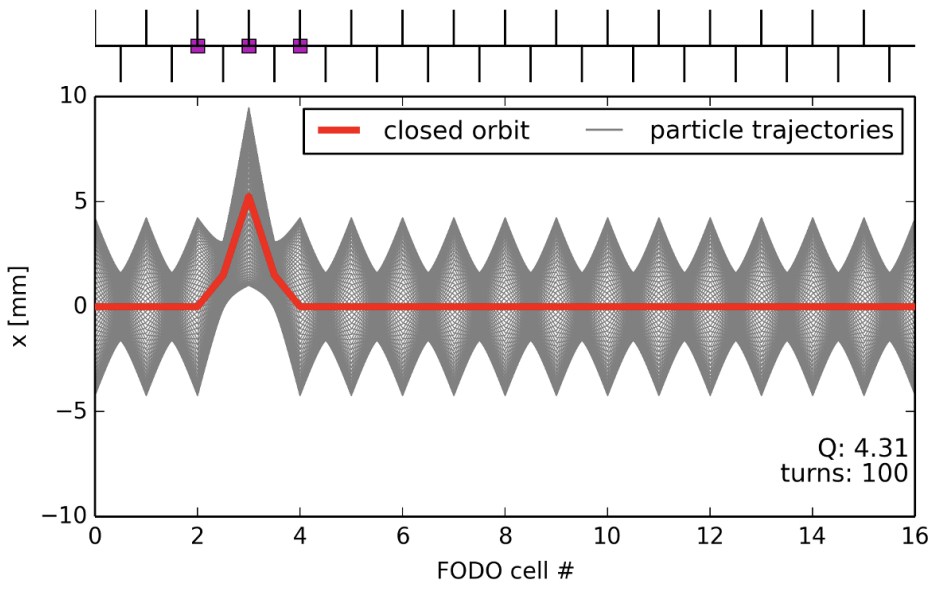

Fig. I.8.15: closed-orbit bump using three correctors. The dipole correctors are indicated in the plot by the purple squares.

The general framework for building local closed-orbit bumps is the following. Consider the trans-

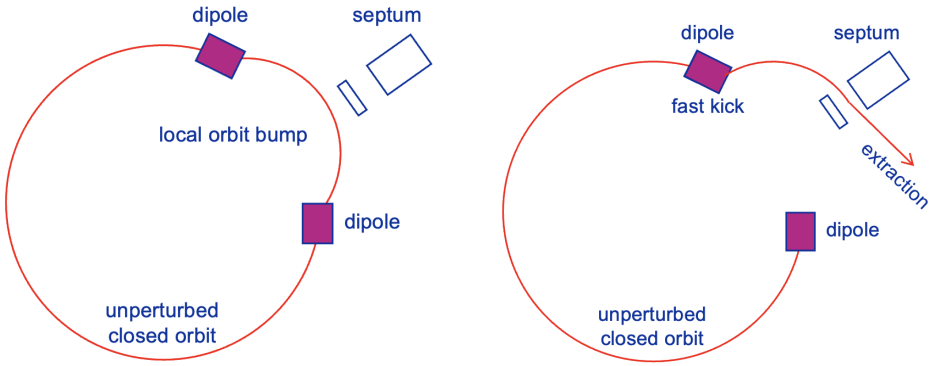

Fig. I.8.16: Schematic representation of an extraction bump using two correctors: before extraction (left) and at extraction (right) where in addition a fast kicker magnet is fired to bring the beam through the extraction septum out of the machine.

port matrix between two positions in an accelerator, here from position 1 to position 2

$$\mathcal{M}_{1\to 2} = \begin{pmatrix} m_{11} & m_{12} \\ m_{21} & m_{22} \end{pmatrix} = \begin{bmatrix} \sqrt{\frac{\beta_2}{\beta_1}}(\cos\psi_{12} + \alpha_1 \sin\psi_{12}) & \sqrt{\beta_2\beta_1}\sin\psi_{12} \\ \frac{\alpha_1-\alpha_2}{\sqrt{\beta_2\beta_1}}\cos\psi_{12} - \frac{1+\alpha_2\alpha_1}{\sqrt{\beta_2\beta_1}}\sin\psi_{12} & \sqrt{\frac{\beta_1}{\beta_2}}(\cos\psi_{12} - \alpha_2\sin\psi_{12}) \end{bmatrix}.$$

Now, consider a single-dipole kick at position 1

$$\theta_1 = \frac{\delta(Bl)}{B\rho}.$$

At position 2, the variation of position (δu_2) and angle $(\delta u_2')$ can be expressed as

$$\begin{pmatrix} \delta u_2 \\ \delta u_2' \end{pmatrix} = \mathcal{M}_{1\to 2} \begin{pmatrix} 0 \\ \theta_1 \end{pmatrix}.$$

Inserting the coefficients from the general betatron matrix, we obtain

$$\delta u_2 = \sqrt{\beta_1\beta_2}\sin(\psi_{12})\theta_1,$$

and

$$\delta u_2' = \sqrt{\frac{\beta_1}{\beta_2}}[\cos(\psi_{12}) - \alpha_2\sin(\psi_{12})]\theta_1.$$

Using these simple formulas, one can calculate the conditions to create local closed-orbit bumps using the desired numbers of correctors. The simplest cases are using between two and four correctors, as depicted in Fig. I.8.17.

Consider a cell in which the correctors are placed close to the focusing quadrupoles. The orbit shift at the second corrector is obtained as

$$\delta u_2 = \sqrt{\beta_1\beta_2}\sin(\psi_{12})\theta_1.$$

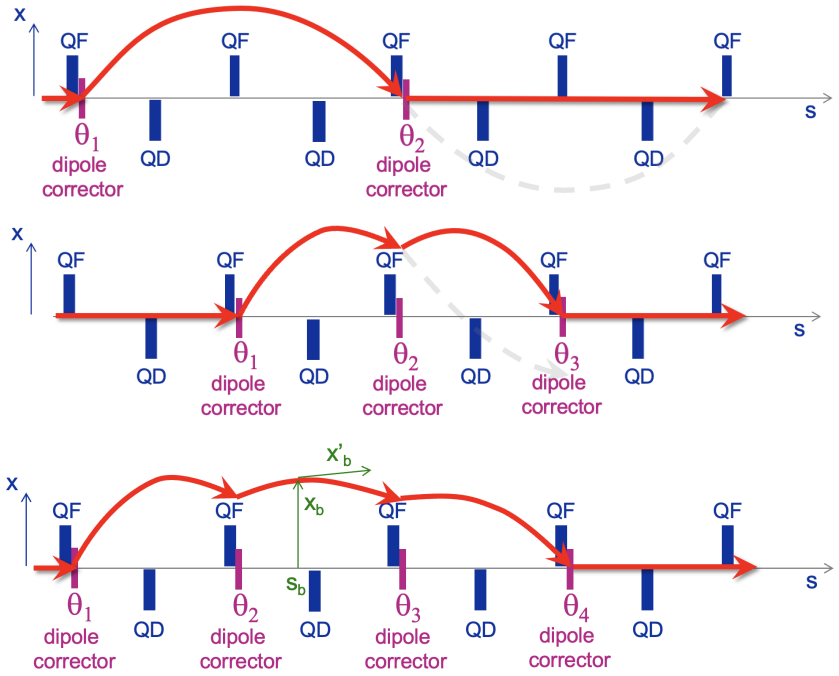

Fig. I.8.17: Diagram of typical orbit bumps using two (top), three (middle) or four (bottom) orbit correctors.

This orbit bump can be closed by choosing a phase advance equal to π between the correctors (this is called a "π-bump"). The kick at position 2 needs to satisfy the following equation

$$\theta_2 = \delta u_2' = -\sqrt{\frac{\beta_1}{\beta_2}}\left[\cos(\psi_{12}) - \alpha_2 \sin(\psi_{12})\right]\theta_1 = \sqrt{\frac{\beta_1}{\beta_2}}\theta_1.$$

The restriction to a phase advance of a multiple of π is unpractical in most situations. Therefore the 3-corrector bump is more commonly used, as it works for any phase advance if the three correctors satisfy certain conditions. The angle of the closed orbit (i.e. the slope of the closed orbit) in the center of the bump is defined by the conditions to achieve a closed bump, and it can thus not be adjusted independently of the bump amplitude. The condition for such a bump to be closed is

$$\frac{\sqrt{\beta_1}}{\sin\psi_{23}}\theta_1 = \frac{\sqrt{\beta_2}}{\sin\psi_{31}}\theta_2 = \frac{\sqrt{\beta_3}}{\sin\psi_{12}}\theta_3. \tag{I.8.40}$$

Note that in the above equation ψ_{23} indicates the phase advance from location 2 to location 3, ψ_{31} indicates the phase advance from location 3 to location 1, and ψ_{12} the phase advance from location 1 to location 2.

Another way to understand two and three orbit corrector bumps is to use normalised phase-space coordinates, as show in Fig. I.8.18. In this illustration, the "π-bump" is obvious, while the three-corrector-bump relation can easily be extracted using the "law of sines" in triangles.

Finally, a four-corrector bump allows for independent adjustment of the position x_b and angle x_b' of the closed-orbit bump at location s_b. This configuration can be used for aperture scanning, extraction

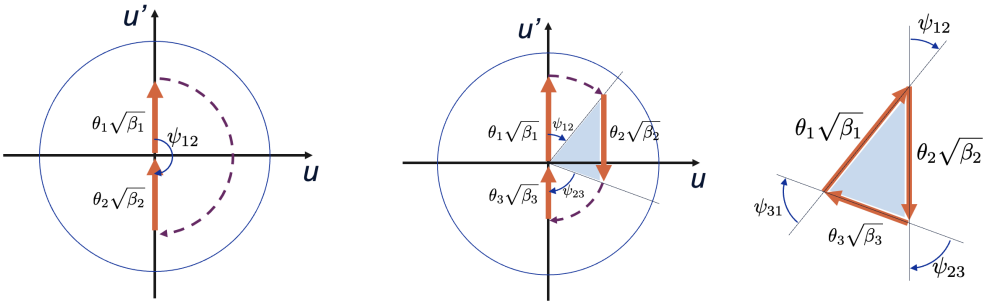

Fig. I.8.18: Phase-space representation of closed-orbit bumps using two (left) or three (right) orbit correctors.

bumps, and more. The derivation of the conditions for achieving a closed bump is more lengthy, but following similar derivations as before one obtains the following equations

$$\theta_1 = +\frac{1}{\sqrt{\beta_1\beta_b}}\frac{\cos\psi_{2b} - \alpha_b\sin\psi_{2b}}{\sin\psi_{12}}x_b - \sqrt{\frac{\beta_b}{\beta_1}}\frac{\sin\psi_{2b}}{\sin\psi_{12}}x'_b, \tag{I.8.41}$$

$$\theta_2 = -\frac{1}{\sqrt{\beta_2\beta_b}}\frac{\cos\psi_{1b} - \alpha_b\sin\psi_{1b}}{\sin\psi_{12}}x_b + \sqrt{\frac{\beta_b}{\beta_2}}\frac{\sin\psi_{1b}}{\sin\psi_{12}}x'_b, \tag{I.8.42}$$

$$\theta_3 = -\frac{1}{\sqrt{\beta_3\beta_b}}\frac{\cos\psi_{b4} + \alpha_b\sin\psi_{b4}}{\sin\psi_{34}}x_b - \sqrt{\frac{\beta_b}{\beta_4}}\frac{\sin\psi_{b4}}{\sin\psi_{34}}x'_b, \tag{I.8.43}$$

$$\theta_4 = +\frac{1}{\sqrt{\beta_4\beta_b}}\frac{\cos\psi_{b3} + \alpha_b\sin\psi_{b3}}{\sin\psi_{34}}x_b + \sqrt{\frac{\beta_b}{\beta_4}}\frac{\sin\psi_{b3}}{\sin\psi_{34}}x'_b. \tag{I.8.44}$$

I.8.2.7.1 Problem 4

Three correctors are placed at locations with a phase advance of $\pi/4$ between them and beta functions of 12, 2, and 12 meters. The question is: how are the corrector kicks related to each other in order to achieve a closed three-corrector bump (i.e., what is the relative strength between the three kicks)?

I.8.2.7.2 Solution to problem 4

- The relations for achieving a three-bump are

$$\frac{\sqrt{\beta_1}}{\sin\psi_{23}}\theta_1 = \frac{\sqrt{\beta_2}}{\sin\psi_{31}}\theta_2 = \frac{\sqrt{\beta_3}}{\sin\psi_{12}}\theta_3.$$

- The phase advances are $\psi_{12} = \psi_{23} = \pi/4$ and $\psi_{13} = \psi_{12} + \psi_{23} = \pi/2$, which gives $\psi_{31} = -\pi/2$.
- So $\theta_1 = \theta_3$ and $\theta_2 = -\theta_1\sqrt{12}$.

I.8.2.8 Closed-orbit correction - global

Global orbit correction is a fundamental process in synchrotrons to ensure that the particle beam follows the desired path as closely as possible. Over time, various methods have been developed to address this problem. One of the most widely used methods at CERN is the MICADO (from French "MInimisation des CArrés des Distortions d'Orbite") algorithm [2], which has been implemented in different programming languages, evolving from FORTRAN to modern languages such as Java, C, and C++.

I.8.2.8.1 MICADO algorithm

The MICADO algorithm, introduced by B. Autin and Y. Marti in 1973 [2], is a deterministic approach to minimizing quadratic orbit distortions. The principle behind MICADO is relatively simple and involves the following steps:

1. A model of the machine is required;
2. The effect (response) of each orbit corrector on the orbit is computed;
3. MICADO compares the response of every corrector with the raw orbit in the machine;
4. The corrector that has the best match with the raw orbit, i.e. the one that will give the largest improvement to the RMS orbit deviation, is selected;
5. The procedure is iterated to include the second-best corrector, and so on, until the orbit is sufficiently corrected or cannot be improved further.

An example application of the MICAOD algorithm to the closed-orbit correction the CERN LHC is shown in Fig. I.8.19.

It should be noted that the intuitive nature of the MICADO algorithm allows it to be applied not only for orbit correction using the measured orbit distortion but also for the correction of other linear effects.

I.8.2.8.2 Singular Value Decomposition - SVD

Another approach for global orbit correction involves using the response matrix, which relates the kicks from correctors to the closed-orbit displacements at BPMs. The steps in this method are as follows:

1. Consider a set of M available orbit correctors and N BPMs;
2. Assume or verify that the linear approximation is sufficient (typicall OK for small corrections);
3. Use the optics model to compute the response matrix A, which describes the orbit change in the i^{th} monitor due to a unit kick from the j^{th} corrector. The elements $A_{i,j}$ of the response matrix A are obtained using the previously defined formalism as

$$A_{i,j} = \frac{\sqrt{\beta_i \beta_j}\cos(\pi Q - |\psi_i - \psi_j|)}{2\sin(\pi Q)}$$

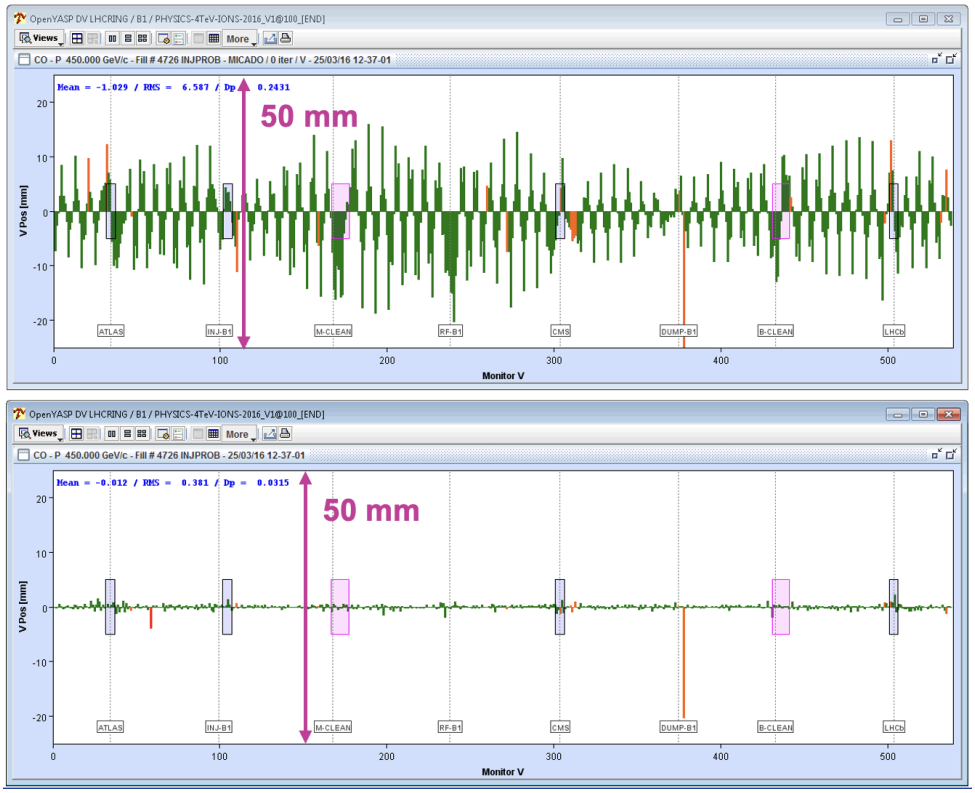

Fig. I.8.19: Example of MICADO orbit correction at the LHC. The raw orbit (top) can have large errors, but the correction brings the deviations down by a factor of 20 (below).

and can be computed using a beam optics simulation program like MAD-X or even measured directly in the machine;

4. To compute the correction to achieve the desired global orbit variation, we invert the response matrix A so that

$$\Delta\mathbf{c} = A^{-1}\Delta\mathbf{m},$$

where $\Delta\mathbf{c}$ are the corrector strengths and $\Delta\mathbf{m}$ are the measured orbit deviations.

When the number of correctors M is not equal to the number of BPMs N, a Singular Value Decomposition (SVD) is used to perform a pseudo-inversion of the response matrix. The SVD algorithm decomposes the response matrix A into three matrices

$$A = U\Sigma V^T,$$

where U and V are orthogonal matrices, Σ is a diagonal matrix containing the singular values and T indicates the transpose of a matrix.

The correction $\Delta\mathbf{c}$ is then computed as

$$\Delta\mathbf{c} = V\Sigma^{-1}U^T\Delta\mathbf{m}.$$

I.8.2.9 Concluding remarks on beam orbit stability

Beam orbit stability is a crucial aspect of the operation of synchrotrons, significantly impacting various performance parameters. Ensuring stable beam orbits is essential for several reasons. Firstly, it directly affects the injection and extraction efficiency of synchrotrons. Any instability in the orbit can lead to losses during these processes, reducing the overall efficiency of the machine. Secondly, in colliders, the stability of the collision point is paramount. Unstable orbits can cause shifts in the collision point, adversely affecting the experimental conditions. Thirdly, for synchrotron light sources, the stability of the light spot in the beamlines is critical for the precision of experiments and the quality of the generated light.

The consequences of orbit distortion are numerous and detrimental. Mis-steering of beams can occur, leading to off-centered orbits that can cause beam losses. Modifications of the dispersion function and resonance excitation can also result from orbit distortions, further complicating beam dynamics. Aperture limitations may be encountered, reducing the operational efficiency and lifetime of the beam. Additionally, orbit distortions can induce coupling between the horizontal and vertical planes of particle motion, modulation of lattice functions, and poor injection/extraction efficiency, all of which degrade the overall performance of the accelerator.

Sources of closed-orbit drifts can be categorized by their timescales. Long-term drifts, occurring over years to months, are often due to ground settling and seasonal changes. These slow drifts can gradually alter the alignment of the accelerator components, necessitating periodic corrections. Medium-term drifts, spanning days to hours, can be caused by various environmental factors such as thermal variations due to the sun, weather changes including rivers, rain, and wind, and operational factors. These drifts can also result from the drift of electronics and local machinery, which require regular monitoring and adjustment. Short-term drifts, happening within minutes to seconds, are primarily due to ground vibrations, fluctuations in power supplies, the influence of experimental magnets, and the operation of air conditioning and refrigeration systems. These rapid changes might necessitate real-time correction mechanisms to maintain orbit stability.

I.8.2.9.1 Problem 5

The SPS is a 400 GeV proton synchrotron with a FODO lattice consisting of 108 focusing and 108 defocusing quadrupoles of length 3.22 m and a gradient of 15 T/m, with horizontal and vertical β functions of 108 m and 30 m in the focusing quadrupoles (30 m and 108 m for the defocusing ones). The tunes are $Q_x = 20.13$ and $Q_y = 20.18$. In 2016, a mechanical problem resulted in the vertical movement of one of the focusing quadrupoles, i.e. it was sinking down, resulting in an increasing closed-orbit distortion compared to a reference closed orbit taken earlier in the year.

a) By how much had the quadrupole shifted down when the maximum vertical closed-orbit distortion amplitude in defocusing quadrupoles reached 4 mm?

b) Why was there no change in the horizontal orbit measured?

c) How big would have been the maximum closed-orbit distortion amplitude if it had been a

defocusing quadrupole?

I.8.2.9.2 Solution to problem 5

a) – For 400 GeV, the relativistic beta is almost 1 and then the magnetic rigidity is

$$B\rho = 3.3356\beta_r E\,[\text{GeV}] = 1334\,\text{Tm}.$$

– The focusing normalized gradient is

$$K_F = \frac{G_F}{B\rho} = \frac{15}{1334} = 0.011\,\text{m}^{-2}$$

– The defocusing one is just the same with opposite sign

$$K_D = -0.011\,\text{m}^{-2}.$$

– The closed-orbit distortion from a single-dipole error is given by

$$u(s) = \theta\frac{\sqrt{\beta(s)\beta_0}}{2\sin(\pi Q)}\cos(\pi Q - |\psi(s) - \psi_0|).$$

– We are interested in the peak ($\hat{y}$) orbit distortion

$$\hat{y} = \theta\frac{\sqrt{\hat{\beta}_y\beta_0}}{2\sin(\pi Q)}.$$

– From this we can calculate the required kick

$$\theta = \frac{\hat{y}2\sin(\pi Q)}{\sqrt{\hat{\beta}_y\beta_0}} = \frac{0.004 \times 2\sin(\pi 20.18)}{\sqrt{108 \times 30}} = 75\,\mu\text{rad}.$$

– And finally the required quadrupole displacement to produce this deflection

$$\theta = \frac{Gl\delta y}{B\rho} = K_F l_F \delta y \quad \Rightarrow \quad \delta y = \frac{\theta}{K_F l_F} = \frac{75 \times 10^{-6}}{0.011 \times 3.22}\,\text{m} = 2\,\text{mm}.$$

b) No horizontal orbit change was observed because the quadrupole shifted only in the vertical plane resulting in a pure vertical kick.

c) If it had been a defocusing quadrupole, the kick would have been the same but with the opposite sign. However, the impact on the closed orbit would have been bigger since the vertical β-function is bigger in the defocusing quadrupole, such that the peak orbit distortion

would reach

$$\hat{y} = \theta \frac{\sqrt{\hat{\beta}_y \beta_0}}{2\sin(\pi Q)} = \theta \frac{\sqrt{\hat{\beta}_y \hat{\beta}_y}}{2\sin(\pi Q)} = 75 \times 10^{-6} \times \frac{\sqrt{108 \times 108}}{2\sin(\pi \times 20.18)}\,\mathrm{m} = 7.5\,\mathrm{mm}.$$

I.8.3 Optics function distortion - gradient errors

Optics errors in synchrotrons can significantly impact the stability and performance of particle beams. These errors lead to phenomena such as tune shifts, beta-beating, and resonance excitation, which can degrade the quality of the beam and affect the overall efficiency of the accelerator. Hence, maintaining control over optics is critical for machine performance, especially at collision points or collimators, such as in the LHC.

A common source of optics errors is the presence of quadrupole errors, i.e. unwanted quadrupolar fields in the accelerator. These result in additional focusing or defocusing of the particle beam. When a particle is injected with an offset, it performs betatron oscillations and experiences additional focusing (or defocusing) from the quadrupole error, leading to a tune shift and beta-beating. The ideal machine model with a regular FODO lattice can be used to illustrate this effect. Consider a quadrupole error located at the end of the lattice, as shown in Fig. I.8.20. The particle's betatron oscillations will be modified by the error, leading to a distorted beam envelope around the machine, commonly referred to as beta-beating. Also note that the quadrupole error has modified the tune of the machine.

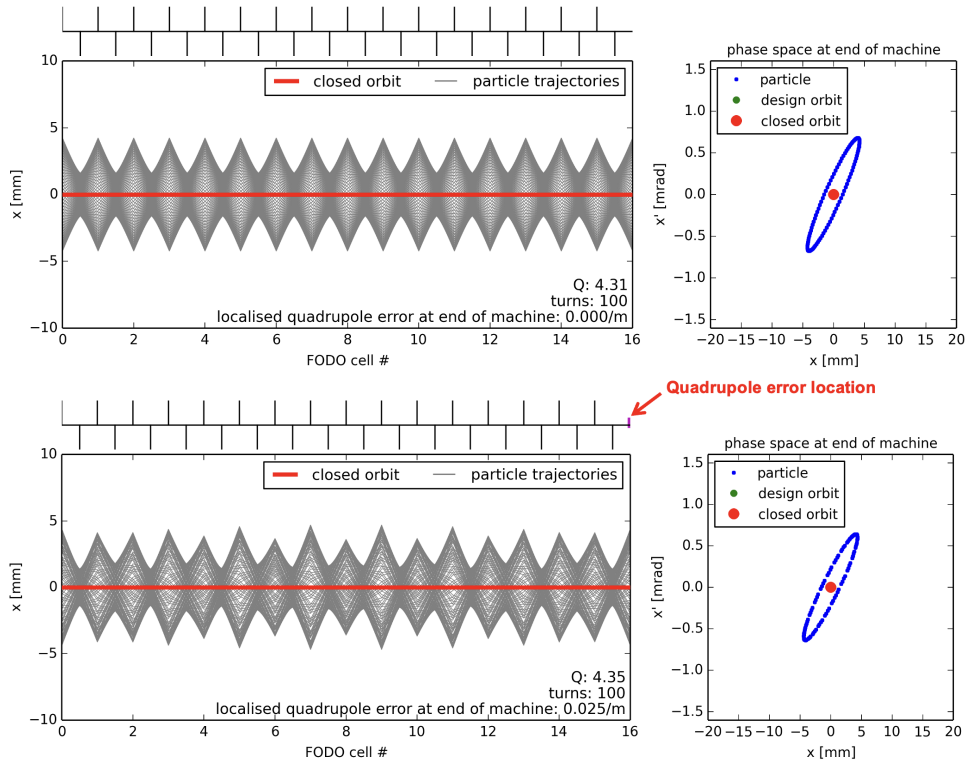

Fig. I.8.20: Illustration of optics distortion, comparing the nominal (top) with the perturbed optics (bottom) for the case of a regular FODO lattice. The quadrupole error results in a distortion of the beam envelope and induces a tune shift (the tunes are indicated in the plots).

Optics errors can arise from various sources, including errors in quadrupole strengths (both random and systematic), stray fields from injection / extraction elements, feed-down from higher order multi-pole magnets and their errors if the beam has a non-zero closed-orbit distortion at their location.

I.8.3.1 Mathematical description of optics errors

First we will investigate how a single quadrupole error changes the tune of the machine. Let's consider the one-turn transfer matrix of the machine

$$M_0 = \begin{pmatrix} \cos(2\pi Q) + \alpha_0 \sin(2\pi Q) & \beta_0 \sin(2\pi Q) \\ -\gamma_0 \sin(2\pi Q) & \cos(2\pi Q) - \alpha_0 \sin(2\pi Q) \end{pmatrix}. \tag{I.8.45}$$

A gradient error δK in a quadrupole can be taken into account by adding a thin-lens quadrupole to the one-turn matrix. The new one-turn matrix is then obtained as

$$M = \begin{pmatrix} 1 & 0 \\ -\delta K ds & 1 \end{pmatrix} M_0, \tag{I.8.46}$$

which yields

$$M = \begin{pmatrix} \cos(2\pi Q) + \alpha_0 \sin(2\pi Q) & \beta_0 \sin(2\pi Q) \\ -\delta K ds(\cos(2\pi Q) + \alpha_0 \sin(2\pi Q)) - \gamma_0 \sin(2\pi Q) & \cos(2\pi Q) - (\delta K ds \beta_0 + \alpha_0) \sin(2\pi Q) \end{pmatrix}. \tag{I.8.47}$$

This one-turn transfer matrix can also be written as a new one-turn transfer matrix

$$M^* = \begin{pmatrix} \cos(\chi) + \alpha_0^* \sin(\chi) & \beta_0^* \sin(\chi) \\ -\gamma_0^* \sin(\chi) & \cos(\chi) - \alpha_0^* \sin(\chi) \end{pmatrix}, \tag{I.8.48}$$

where $\chi = 2\pi(Q + \delta Q)$ denotes the new tune of the new matrix. These two one-turn matrices are equal as they describe the same machine. Thus, also the traces of these matrices have to be equal, i.e. trace$(M) =$ trace(M_0), which gives

$$2\cos(2\pi Q) - \delta K ds \beta_0 \sin(2\pi Q) = 2\cos(2\pi(Q + \delta Q)). \tag{I.8.49}$$

Developing the right-hand side as

$$\cos(2\pi(Q + \delta Q)) = \cos(2\pi Q)\cos(2\pi \delta Q) - \sin(2\pi Q)\sin(2\pi \delta Q) \approx \cos(2\pi Q) - \sin(2\pi Q) 2\pi \delta Q, \tag{I.8.50}$$

and inserting it back finally results in the tune shift induced by a thin-lens quadrupole

$$4\pi \delta Q = \delta K ds \beta_0. \tag{I.8.51}$$

For a quadrupole of length l the tune shift is thus

$$\delta Q = \frac{1}{4\pi} \int_{s_0}^{s_0+l} \delta K(s) \beta(s) ds, \tag{I.8.52}$$

and more generally for distributed quadrupole errors, the tune shift is obtained as

$$\delta Q = \frac{1}{4\pi} \oint \delta K(s)\beta(s)ds. \tag{I.8.53}$$

In the following, we will investigate the optics distortion induced by a quadrupole error in the machine. Here we consider the unperturbed transfer matrix for one turn M_0 written as the product of two transport matrices A and B

$$M_0 = \begin{pmatrix} m_{11} & m_{12} \\ m_{21} & m_{22} \end{pmatrix} = B \cdot A, \tag{I.8.54}$$

with

$$A = \begin{pmatrix} a_{11} & a_{12} \\ a_{21} & a_{22} \end{pmatrix} \quad \text{and} \quad B = \begin{pmatrix} b_{11} & b_{12} \\ b_{21} & b_{22} \end{pmatrix}. \tag{I.8.55}$$

Introducing a thin-lens quadrupole representing a gradient perturbation between the two matrices A and B allows to obtain the perturbed one-turn transfer matrix as

$$M_0^* = \begin{pmatrix} m_{11}^* & m_{12}^* \\ m_{21}^* & m_{22}^* \end{pmatrix} = B \begin{pmatrix} 1 & 0 \\ -\delta K ds & 1 \end{pmatrix} A. \tag{I.8.56}$$

Recalling that $m_{12} = \beta_0 \sin(2\pi Q)$ we can write the perturbed term as

$$m_{12}^* = (\beta_0 + \delta\beta)\sin(2\pi(Q + \delta Q)) = m_{12} + \delta\beta \sin(2\pi Q) + 2\pi\delta Q\beta_0 \cos(2\pi Q), \tag{I.8.57}$$

where we used $\sin(2\pi\delta Q) \approx 2\pi\delta Q$ and $\cos(2\pi\delta Q) \approx 1$, as well as

$$\sin(2\pi(Q + \delta Q)) = \sin(2\pi Q)\cos(2\pi\delta Q) + \cos(2\pi Q)\sin(2\pi\delta Q). \tag{I.8.58}$$

On the other hand, the matrices A and B have the coefficients $a_{12} = \sqrt{\beta_0\beta(s_1)}\sin\psi$ and $b_{12} = \sqrt{\beta_0\beta(s_1)}\sin(2\pi Q - \psi)$ and we can thus write the perturbed matrix element m_{12}^* explicitly as

$$m_{12}^* = b_{11}a_{12} + b_{12}a_{22} - a_{12}b_{12}\delta K ds = m_{12} - a_{12}b_{12}\delta K ds. \tag{I.8.59}$$

Combining Eqs. (I.8.57) and (I.8.59) yields

$$\delta\beta \sin(2\pi Q) + 2\pi\delta Q\beta_0 \cos(2\pi Q) = -\beta_0\beta(s_1)\sin\psi \sin(2\pi Q - \psi)\delta K ds, \tag{I.8.60}$$

and inserting for δQ the expression from Eq. (I.8.51), we obtain

$$\delta\beta \sin(2\pi Q) + \frac{1}{2}\delta K ds \beta_0\beta(s_1)\cos(2\pi Q) = -\beta_0\beta(s_1)\sin\psi \sin(2\pi Q - \psi)\delta K ds. \tag{I.8.61}$$

Using

$$\cos A - \cos B = -2\sin\left(\frac{A+B}{2}\right)\sin\left(\frac{A-B}{2}\right) \tag{I.8.62}$$

yields the expression for the relative beta distortion

$$\frac{\delta\beta}{\beta_0} = -\frac{1}{2\sin(2\pi Q)} \int_{s_1}^{s_1+C} \beta(s)\delta K(s)\cos(2\psi - 2\pi Q)ds. \tag{I.8.63}$$

For distributed errors around the machine we obtain

$$\frac{\delta\beta(s)}{\beta(s)} = -\frac{1}{2\sin(2\pi Q)} \int_{s}^{s+C} \beta(s_1)\delta K(s_1)\cos(|2\psi(s_1) - 2\psi(s)| - 2\pi Q)ds_1. \tag{I.8.64}$$

This equation shows how the gradient error perturbs the beta function around the ring. Note that the impact of a quadrupole error on the tune and on the optics distortion (beta-beating) scales with the β function at the location of the quadrupole error. The induced beta-beating wave propagates with twice the lattice phase advance around the machine (due to the term $2\psi(s)$ in the cosine). Furthermore, the expression for the beta-beating shows that quadrupole errors have the biggest impact close to integer and half-integer tunes due to the $\sin(2\pi Q)$ in the denominator. At these resonances the beam envelope (or the beam size) becomes unstable.

For machine operation, it is thus essential to avoid not only integer but also half-integer tunes. Similar to the case of dipole errors, at integer tunes also the kicks from quadrupole errors add up turn after turn resulting in unstable motion (dipole errors result in an unstable closed orbit, quadrupole errors in unstable beam size). Furthermore, at half-integer tunes the quadrupole errors also add up turn after turn (recall that dipole errors have the least impact for half-integer tunes, as they cancel out turn after turn). This is illustrated in Fig. I.8.21.

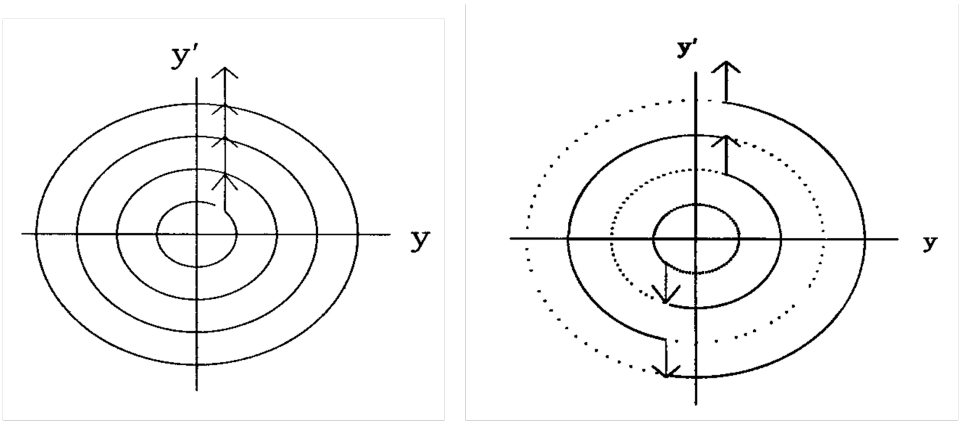

Fig. I.8.21: Effect of a quadrupole error at integer (left) and half-integer (right) tunes. In both cases the errors add up turn after turn, driving the beam envelope unstable.

The example shown in Fig. I.8.22 demonstrates the importance of choosing the machine tune to ensure the robustness of an optics against quadrupole imperfections. The same quadrupole error installed in the FODO lattice with a tune of 4.24 has no noticeable effect on the beam optics around the machine, while for a tune of 4.49 the beam envelope becomes very large and completely distorted, a situation to be avoided in machine operation.

Figure I.8.23 (top) shows a practical example of optics distortion due to quadrupole errors in the

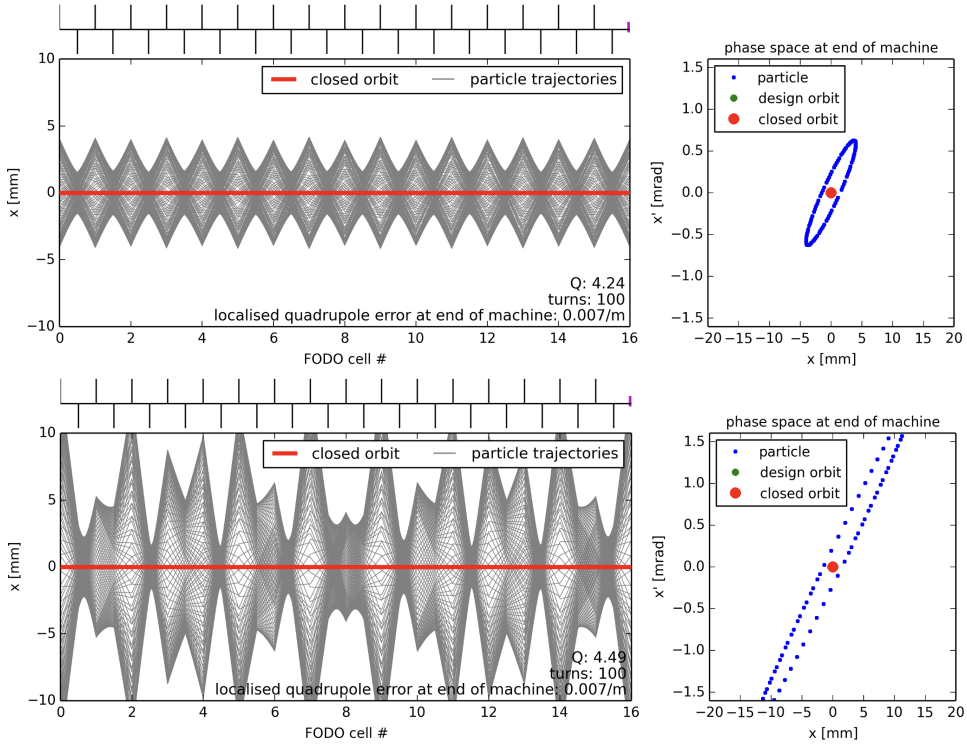

Fig. I.8.22: Illustration of the impact of a quadrupole error on the machine optics. The same quadrupole error is installed in the FODO lattice set to a tune of 4.24 (top) and set to a tune of 4.49 (bottom).

LHC. Compared to the regular β functions in the unperturbed optics, a quadrupole gradient error leads to noticeable perturbations in the β function, resulting in the oscillating pattern. The error is easier to analyse and diagnose if one examines the ratio between the perturbed and the nominal β function when plotted against the betatron phase advance as shown in Fig. I.8.23 (bottom). The β function ratio reveals an oscillating pattern, called the betatron function beating ('beta-beating'). The amplitude of the perturbation is the same all over the ring. Similar to the case of the closed-orbit kick, the location of the quadrupole error reveals itself by a kink in the oscillation pattern. Furthermore, it can be easily seen that there are two oscillation periods per 2π (360 deg) phase advance. The beta-beating frequency is twice the frequency of orbit oscillations.

I.8.3.2 Correction and mitigation of optics distortion due to quadrupole errors

Understanding and mitigating the impact of optics errors is crucial for maintaining the stability and performance of synchrotrons. Through careful analysis and correction of these errors, it is possible to minimize their adverse effects and ensure optimal machine operation. Quadrupole correctors can be foreseen in the machine design to mitigate the effects of gradient errors. These correctors can take several forms:

- **Individual correction magnets:** these are dedicated magnets placed at strategic locations around the synchrotron to correct gradient errors (locally or globally).
- **Windings on the core of the quadrupoles (trim windings):** additional windings are integrated into the quadrupole magnets, allowing fine-tuning of the magnetic field to correct errors.

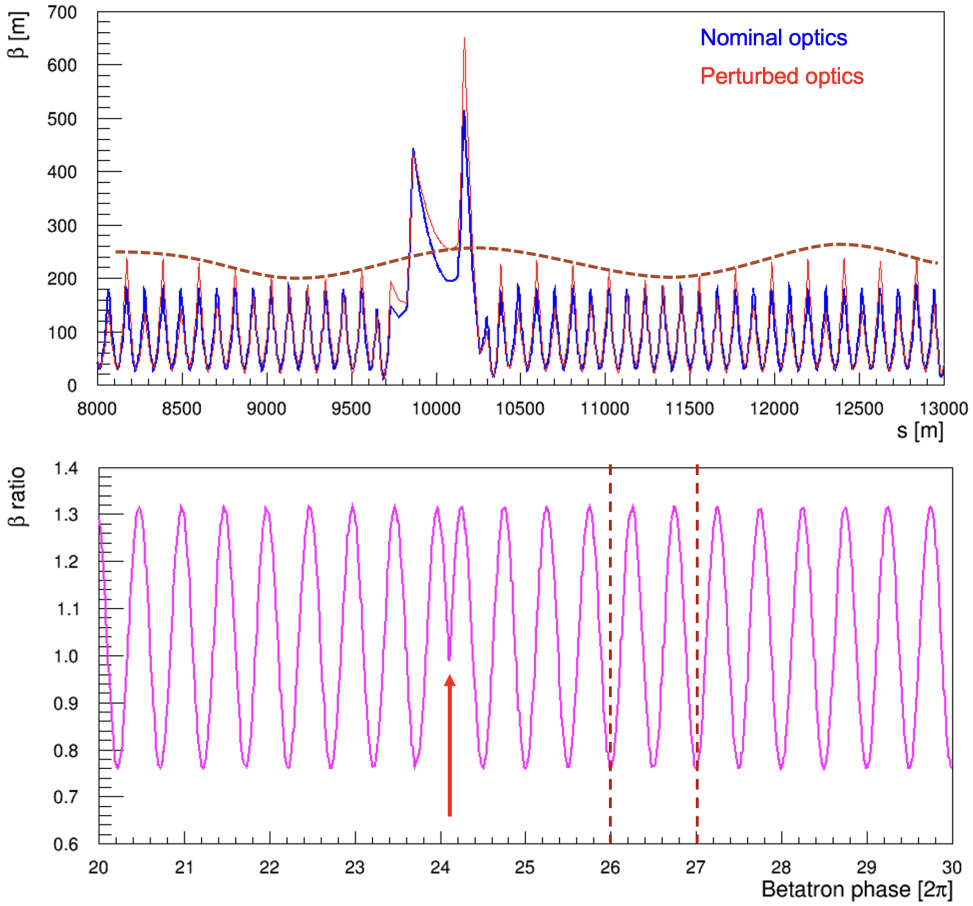

Fig. I.8.23: Example of a perturbed β function within a segment of the LHC ring. The top plot displays the nominal and perturbed optics as a function of the longitudinal position in the ring. The bottom plot illustrates the ratio of perturbed to nominal optics as a function of phase advance. Notice the kink in the oscillatory pattern, indicating the location of the source of the optics perturbation, and the frequency of the oscillation in the rest of the ring, which is twice the frequency of the phase advance.

– **Pairs of correctors at well-chosen locations:** corrector pairs can be installed to minimize resonance effects.

Several methods and approaches are available to address the impact of gradient errors:

– **Measuring and correcting the optics function β distortion:** the β function distortion can be obtained by analysing the betatron motion of a kicked beam at various BPMs around the machine. The most commonly used technique is based on reconstructing the beta-beating from the measured phase beating of the betatron motion between BPMs. This method is usually the preferred option, as it does not rely on the BPM calibration (unlike the analysis based on the direct measurement of the oscillation amplitude between BPMs). Suitable corrections can be determined through a response matrix approach, similar to what was discussed in the context of closed-orbit corrections (SVD).

– **Move the working point close to integer and half-integer resonance:** adjusting the working point to be near these resonances can increase the sensitivity to quadrupole errors, which can be

useful when the optics correction aims at minimizing the half-integer resonance strength.

– **Individual powering of quadrupoles and/or trim windings:** individual powering of a quadrupole allows direct measurement of optics functions at the location of the quadrupole by exploiting Eq. (I.8.52), which is the so called K-modulation technique. The β function is directly related to the measured tune shift when varying the strength of the quadrupole. Furthermore, individually powered quadrupoles allow for optics correction as well as beam-based alignment of BPMs.

Modern methods of response matrix analysis, such as Linear Optics from Closed Orbits (LOCO), play a crucial role in fitting the optics model to the real machine and correcting optics distortion, especially for light sources for which the machine performance (i.e. the resulting equilibrium emittance) depends crucially on the control of the machine optics. LOCO works by analyzing the response of the beam to various magnetic configurations and deriving corrections that align the actual machine behaviour with the theoretical model.

I.8.3.2.1 Problem 6

The SPS is a 400 GeV proton synchrotron with a FODO lattice consisting of 108 focusing and 108 defocusing quadrupoles, each with a length of 3.22 m and a gradient of 15 T/m, with a horizontal and vertical β function of 108 m and 30 m in the focusing quadrupoles (30 m and 108 m for the defocusing ones). The tunes are $Q_x = 20.13$ and $Q_y = 20.18$.

a) Find the tune shift for systematic gradient errors of +1% in the focusing and +0.5% in the defocusing quadrupoles.

b) Find the β_x and β_y rms beating for rms gradient errors of 1% in both focusing and defocusing quadrupoles.

I.8.3.2.2 Solution to problem 6

a)
– For 400 GeV, the magnetic rigidity is $B\rho = 3.3356\beta_r E\,[\text{GeV}] = 1334\,\text{Tm}$.

– The focusing and defocusing normalized gradients are

$$K_F = \frac{G_F}{B\rho} = \frac{15}{1334} = 0.011\,\text{m}^{-2},\ K_D = -0.011\,\text{m}^{-2}.$$

– Now, the total tune change is given by

$$\delta Q_u = \frac{1}{4\pi}\sum_i \beta_u K_i \left(\frac{\delta K}{K}\right)_i l_i, \text{ with } u = x, y.$$

– By splitting the focusing and defocusing quads, we have

$$\delta Q_u = \frac{1}{4\pi}\left(N_F\beta_u^F K_F\left(\frac{\delta K}{K}\right)_F l_F + N_D\beta_u^D K_D\left(\frac{\delta K}{K}\right)_D l_D\right).$$

– As $N_F = N_D = N$, $l_F = l_D = l$ and $K_F = -K_D = K$, the tune shift can be rewritten as

$$\delta Q_{x,y} = \frac{1}{4\pi}NlK\left(\pm\beta_{x,y}^F\left(\frac{\delta K}{K}\right)_F \mp \beta_{x,y}^D\left(\frac{\delta K}{K}\right)_D\right).$$

– This gives a horizontal and vertical tune shift of

$$\delta Q_x = \frac{108\times 3.22\times 0.011}{4\pi}\left(108\times 0.01 - 30\times 0.005\right) = 0.3, \tag{I.8.65}$$

$$\delta Q_y = \frac{108\times 3.22\times 0.011}{4\pi}\left(-30\times 0.01 + 108\times 0.005\right) = 0.07. \tag{I.8.66}$$

b) – In a similar way, one can compute the **rms beta beating** in case of rms error of 1% for both focusing and defocusing quadrupoles (note that in this case, all signs are positive!). The rms beta beating is given by

$$\left.\frac{\delta\beta_u}{\beta_{0_u}}\right|_{\text{rms}} = \frac{1}{2\sqrt{2}|\sin(2\pi Q)|}\left(\sum_i \delta K_i^2\beta_{u,i}i^2\right)^{1/2}, \tag{I.8.67}$$

$$= \frac{1}{2\sqrt{2}|\sin(2\pi Q_u)|}\sqrt{N}\left|lK\left(\frac{\delta K}{K}\right)\right|\left[\left(\beta_u^F\right)^2 + \left(\beta_u^D\right)^2\right]^{1/2}, \tag{I.8.68}$$

$$= \frac{\sqrt{108}\times 3.22\times 0.011\times 0.01\times\sqrt{108^2+30^2}}{2\sqrt{2}|\sin(2\pi Q_u)|}, \tag{I.8.69}$$

i.e.:

$$\left(\frac{\delta\beta_x}{\beta_{0_x}}\right)_{\text{rms}} = 20\%, \tag{I.8.70}$$

$$\left(\frac{\delta\beta_x}{\beta_{0_x}}\right)_{\text{rms}} = 16\%. \tag{I.8.71}$$

I.8.4 Coupling errors

The beam dynamics in the two transverse planes is coupled if the betatron motion in one plane affects the betatron motion in the other plane. This leads to complications, as the two planes cannot be controlled independently. Linear coupling may result from the rotation of a quadrupole (*tilt*), which introduces a skew-quadrupole component into the magnetic field, as shown in the schematics in Fig. I.8.24.

Similarly, a systematic vertical offset in a sextupole generated through closed-orbit distortion or a vertical misalignment of the magnet also introduces a skew-quadrupole field. In this situation, the magnetic fields can be described as follows

$$B_x = 2B_2x\bar{y} = 2B_2xy + 2B_2x\delta y, \tag{I.8.72}$$

$$B_y = B_2(x^2 - \bar{y}^2) = -2B_2y\delta y + B_2(x^2 - y^2) - B_2(\delta y)^2, \tag{I.8.73}$$

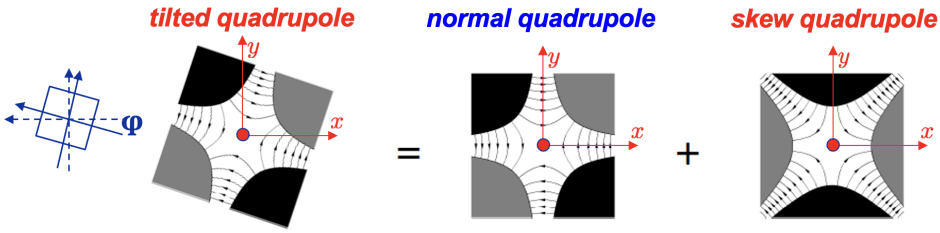

Fig. I.8.24: The magnetic field of tilted quadrupole is equivalent to the sum of normal quadrupole and a skew quadrupole.

where δy represents the vertical offset and $\bar{y}$ is introduced to represent our usual change of variable $\bar{y} = y + \delta y$.

To understand how the skew-quadrupole field induces coupling, let's have a look at the forces generated by a normal and a skew-quadrupole field: Normal quadrupoles produce magnetic fields which result in Lorentz forces that depend on the particle's position in the same plane

$$F_x = -kx, \quad F_y = +ky.$$

In contrast, skew quadrupoles produce magnetic fields which result in Lorentz forces that depend on the position in the orthogonal plane

$$F_x = k_s y, \quad F_y = k_s x.$$

These skew-quadrupole components thus couple the motion in the two planes, leading to cross-talk between horizontal and vertical beam dynamics.

Mathematically, coupling can also be treated using the transport matrix formalism. Starting from the case of uncoupled motion, the transport matrices for each transverse plane can be written separately. Let's consider again the one turn matrix for a given plane u

$$\mathbf{M_u} = \begin{bmatrix} \cos(2\pi Q_u) + \alpha_u \sin(2\pi Q_u) & \beta_u \sin(2\pi Q_u) \\ -\frac{1+\alpha_u^2}{\beta_u} \sin(2\pi Q_u) & \cos(2\pi Q_u) - \alpha_u \sin(2\pi Q_u) \end{bmatrix}.$$

By definition, $\mathbf{M_u}$ is symplectic (see linear dynamics lectures), and as such can be diagonalized in a matrix with elements equal to its eigenvalues (λ_1, λ_2), which must fulfil $\lambda_1 \lambda_2 = 1$, in particular

$$\det(\mathbf{M_u} - \lambda \mathbb{I}) = [\cos(2\pi Q_u) - \lambda]^2 - \alpha_u^2 \sin^2(2\pi Q_u) + (1 + \alpha_u^2) \sin^2(2\pi Q_u) \tag{I.8.74}$$

$$= \lambda^2 - 2\lambda \cos(2\pi Q_u) + 1 = 0 \tag{I.8.75}$$

hence,

$$\lambda_{1/2} = \cos(2\pi Q_u) \pm i \sin(2\pi Q_u) = e^{\pm i 2\pi Q_u} \tag{I.8.76}$$

, which satisfy $\lambda_1 \lambda_2 = 1$. With a transformation $\mathbf{E_u}$ built by the normalized eigenvectors of $\mathbf{M_u}$ one can

diagonalize the latter

$$\mathbf{E_u}^{-1}\mathbf{M_u}\mathbf{E_u} = \begin{pmatrix} e^{+i2\pi Q_u} & 0 \\ 0 & e^{-i2\pi Q_u} \end{pmatrix} \tag{I.8.77}$$

, which is equal to the diagonalized version of a simple rotation. Note that this is the case only because the considered matrix $\mathbf{M_u}$ is by construction representing a periodic lattice which has a closed solution. In general, for a generic transport matrix $\mathbf{M_{s_0 s}}$ between two locations of a ring or a transfer line, i.e.

$$\mathbf{M_{s_0,s}} = \begin{bmatrix} \sqrt{\frac{\beta_s}{\beta_{s_0}}}(\cos\psi_{s_0,s} + \alpha_{s_0}\sin\psi_{s_0,s}) & \sqrt{\beta_s\beta_{s_0}}\sin\psi_{s_0,s} \\ \frac{\alpha_{s_0}-\alpha_s}{\sqrt{\beta_s\beta_{s_0}}}\cos\psi_{s_0,s} - \frac{1+\alpha_s\alpha_{s_0}}{\sqrt{\beta_s\beta_{s_0}}}\sin\psi_{s_0,s} & \sqrt{\frac{\beta_{s_0}}{\beta_s}}(\cos\psi_{s_0,s} - \alpha_s\sin\psi_{s_0,s}) \end{bmatrix} \tag{I.8.78}$$

the eigenvalues would still need to fulfill the relation $\lambda_1\lambda_2 = 1$, but the amplitude of one of the two eigenvalues could be greater than one, which would not correspond anymore to a rotation, but representing an un-bounded lattice.

So far, we have considered each plane independently, meaning the coordinates of a particle at a given location are transported from turn n to the turn after $n+1$ as follows

$$\begin{pmatrix} x \\ x' \end{pmatrix}_{n+1} = \mathbf{M_x}\begin{pmatrix} x \\ x' \end{pmatrix}_n \quad \text{and} \quad \begin{pmatrix} y \\ y' \end{pmatrix}_{n+1} = \mathbf{M_y}\begin{pmatrix} y \\ y' \end{pmatrix}_n \tag{I.8.79}$$

. We can also merge the two 2×2 independent matrices $\mathbf{M_u}$ into a 4×4 block matrix $\mathbf{M}$

$$\begin{pmatrix} x \\ x' \\ y \\ y' \end{pmatrix}_{n+1} = \mathbf{M}\begin{pmatrix} x \\ x' \\ y \\ y' \end{pmatrix}_n = \begin{bmatrix} \mathbf{M_x} & 0 \\ 0 & \mathbf{M_y} \end{bmatrix}\begin{pmatrix} x \\ x' \\ y \\ y' \end{pmatrix}_n = \begin{bmatrix} C_x & S_x & 0 & 0 \\ C'_x & S'_x & 0 & 0 \\ 0 & 0 & C_y & S_y \\ 0 & 0 & C'_y & S'_y \end{bmatrix}\begin{pmatrix} x \\ x' \\ y \\ y' \end{pmatrix}_n . \tag{I.8.80}$$

This formulation represents uncoupled motion, indicating no cross-talk between planes.

The matrix $\mathbf{M}$ must also be symplectic, hence can be diagonalized by a transformation $\mathbf{E}$ in its eigenvalues, which, by virtue of the block composition of $\mathbf{M}$, are equal to the eigenvalues of the individual $\mathbf{M_u}$

$$\mathbf{E}^{-1}\mathbf{M}\mathbf{E} = \begin{bmatrix} e^{+i2\pi Q_x} & 0 & 0 & 0 \\ 0 & e^{-i2\pi Q_x} & 0 & 0 \\ 0 & 0 & e^{+i2\pi Q_y} & 0 \\ 0 & 0 & 0 & e^{-i2\pi Q_y} \end{bmatrix} . \tag{I.8.81}$$

This matrix is equal to the diagonalized version of a simple rotation, with independent rotations in the x and y planes.

Let's now introduce one skew quadrupole, represented by $\mathbf{M_{sq}}$, and built in analogy to the normal

quadrupole matrix in thin-lens approximation. The particle coordinates at turn $n+1$ can be expressed as

$$\begin{pmatrix} x \\ x' \\ y \\ y' \end{pmatrix}_{n+1} = \mathbf{M_{sq}M} \begin{pmatrix} x \\ x' \\ y \\ y' \end{pmatrix}_{n} = \begin{bmatrix} 1 & 0 & 0 & 0 \\ 0 & 1 & 0 & -\delta k_{sq} \\ 0 & 0 & 1 & 0 \\ 0 & -\delta k_{sq} & 0 & 1 \end{bmatrix} \begin{bmatrix} C_x & S_x & 0 & 0 \\ C'_x & S'_x & 0 & 0 \\ 0 & 0 & C_y & S_y \\ 0 & 0 & C'_y & S'_y \end{bmatrix} \begin{pmatrix} x \\ x' \\ y \\ y' \end{pmatrix}_{n} \tag{I.8.82}$$

$$= \begin{bmatrix} C_x & S_x & 0 & 0 \\ C'_x & S'_x & -\delta k_{sq} C_y & -\delta k_{sq} S_y \\ -\delta k_{sq} C_x & -\delta k_{sq} S_x & C_y & S_y \\ 0 & 0 & C'_y & S'_y \end{bmatrix} \begin{pmatrix} x \\ x' \\ y \\ y' \end{pmatrix}_{n} . \tag{I.8.83}$$

Note that the new matrix is not anymore block diagonal, but there are terms in the off-diagonal 2×2 blocks that couple the motion between the two planes. Still, the new matrix must be symplectic and it can be diagonalized in its eigenvalues λ_j, which must also come in pairs such that $\lambda_1 \lambda_2 = 1$ and $\lambda_3 \lambda_4 = 1$. Note that in this case it must also hold $\lambda_1 + \frac{1}{\lambda_1} = \lambda_1 + \lambda_2$ and $\lambda_3 + \frac{1}{\lambda_3} = \lambda_3 + \lambda_4$. Solving $\det(\mathbf{M_{sq}M} - \lambda \mathbf{I}) = 0$, one can get the following relation [3]

$$\lambda + \frac{1}{\lambda} = \cos(2\pi Q_x) + \cos(2\pi Q_y) \pm \sqrt{[\cos(2\pi Q_x) - \cos(2\pi Q_y)]^2 + \delta k_{sq}^2 \beta_x \beta_y \sin(2\pi Q_x) \sin(2\pi Q_y)}. \tag{I.8.84}$$

If the particle motion is still bounded (which is not necessarily the case!) λ must assume the form $\lambda = e^{i2\pi\mu}$, hence

$$\lambda + \frac{1}{\lambda} = e^{i2\pi\mu} + e^{-i2\pi\mu} = 2\cos(2\pi\mu), \tag{I.8.85}$$

where $\mu \in \mathbb{R}$. In analogy with the uncoupled case, one can compute the transformation that diagonalizes the coupled matrix into two independent "tunes" (μ_+, μ_-) which depend on the two uncoupled tunes (Q_x, Q_y)

$$2\cos(2\pi\mu) = \cos(2\pi Q_x) + \cos(2\pi Q_y) \pm \sqrt{[\cos(2\pi Q_x) - \cos(2\pi Q_y)]^2 + \delta k_{sq}^2 \beta_x \beta_y \sin(2\pi Q_x) \sin(2\pi Q_y)}. \tag{I.8.86}$$

In the limit where $Q_x = Q_y := \mu_0$ in Eq. I.8.86, one finds that $\cos(2\pi\mu_+) - \cos(2\pi\mu_-) = \sqrt{\beta_x \beta_y} |\delta k_{sq}| \sin(2\pi\mu_0)$, and if $(\mu_+ - \mu_-) = \Delta\mu$ is small, one can easily prove that $\cos(2\pi\mu_+) - \cos(2\pi\mu_-) \approx \sin(2\pi\mu_0) 2\pi\Delta\mu$, hence

$$\Delta\mu = \mu_+ - \mu_- \approx \frac{\sqrt{\beta_x \beta_y}}{2\pi} |\delta k_{sq}|.$$

This represents the minimum separation between eigenvalues, or, in practice, the minimum tune separation that one could observe in an accelerator, also called the "closest tune approach" (ΔQ_{min}).

Numerically, let's assume to insert the skew quadrupoles at a location where $\beta_x = \beta_y = 1$ and assume $Q_y = 0.25$. For this simplified case, the eigenvalues (μ_+, μ_-) as a function of varying Q_x for

different values of $|\delta k_{sq}|$ are shown in Fig. I.8.25. These plots illustrate the relationship between Q_x and

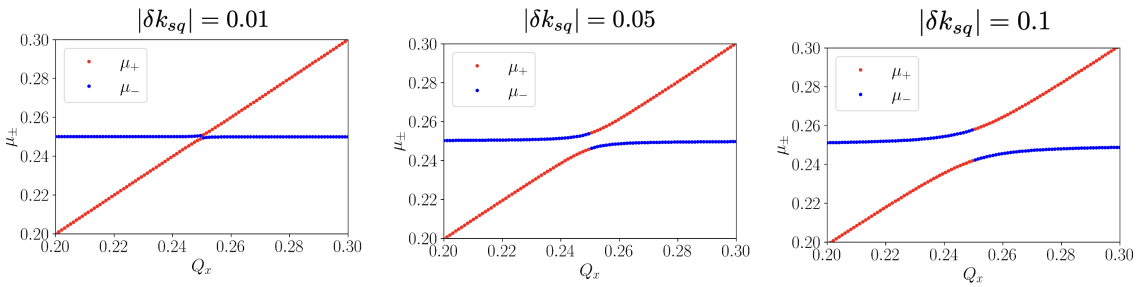

Fig. I.8.25: Coupling eigenvalues for a simplified lattice with a single skew quadruple installed at $\beta_x = \beta_y = 1$ and integrated strength $|\delta k_{sq}| = 0.01$ (left), $|\delta k_{sq}| = 0.05$ (middle), $|\delta k_{sq}| = 0.1$ (right) as a function of the set bare horizontal tune Q_x and fixed bare vertical tune $Q_y = 0.25$.

the eigen-mode tunes for varying strengths of the skew quadrupole. Note the minimum distance between eigenvalues is indeed realized for $Q_x = Q_y = 0.25$ and follows from Eq. I.8.4.

One should also note, using Eq. I.8.86, that in a working point region "close to" $Q_x + Q_y = n$ where $n \in \mathbb{N}$ the particle motion becomes un-bounded. For example, in the limit case $Q_y = 1 - Q_x$ Eq. I.8.86 becomes

$$2\cos(2\pi\mu) = 2\cos(2\pi Q_x) \pm i\sqrt{\beta_x\beta_y}|\delta k_{sq}|\sin(2\pi Q_x),$$

which does not allow any real solution for μ. This can also be demonstrated numerically in a simplified lattice where the skew quadrupole is again inserted at a location where $\beta_x = \beta_y = 1$, and by computing the amplitude of the eigenvalues of $\mathbf{M_{sq}M}$ as a function of (Q_x, Q_y) for different $|\delta k_{sq}|$. The working point regions where at least one eigenvalue has an amplitude greater than 1 indicate where the motion is not stable, as shown in Fig. I.8.26. Note how the "unstable" band around $Q_y = 1 - Q_x$ quickly becomes

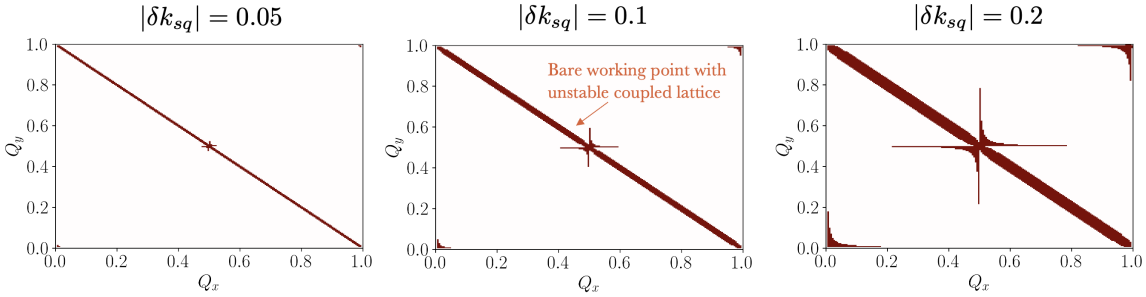

Fig. I.8.26: Unstable regions in the tune diagram for a simplified lattice with a single coupling error inserted at a location where $\beta_x = \beta_y = 1$ and integrated strength $|\delta k_{sq}| = 0.05$ (left), $|\delta k_{sq}| = 0.1$ (middle), $|\delta k_{sq}| = 0.2$ (right).

larger for higher coupling error strength, underlining the importance of having a good control of coupling errors in an accelerator.

In practice, in a real accelerator there might be multiple known and unknown sources of coupling. No unique treatment of this complex problem is available in the literature, but the most common ones are Mais-Ripken [4] and Edwards-Teng [5]. In practice, there is a general consensus that the most

important task remains the estimation of the global coupling coefficient $|C^-|$ and its minimisation. A recent overview of different ways to estimate $|C^-|$ is available in [6].

In a real accelerator the simplest method to determine if there is coupling is to excite a beam oscillation in one plane (e.g. with a fast single kick) and observe the oscillations (e.g. with a turn-by-turn BPM) or the frequency content in the orthogonal plane. If coupling is present, a horizontal kick will produce a small vertical oscillation and vice versa, as shown for example in Fig. I.8.27 for a measurement in the LHC.

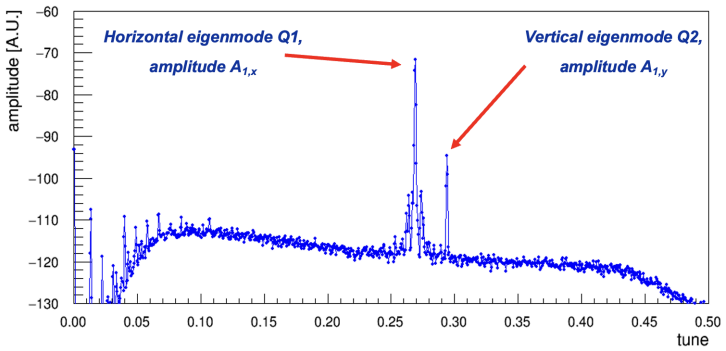

Fig. I.8.27: Spectrum of the horizontal motion measured at one fast transverse pickup in the LHC in the presence of coupling. Mind the logarithmic scale, and the presence of a high-amplitude peak (supposedly close to the bare horizontal tune) and a low-amplitude one (supposedly close to the vertical tune).

To be stressed that, strictly speaking, in this case one does not see the bare tunes (Q_x, Q_x) of the un-coupled motion, but one is measuring the two eigenvalues (μ_+, μ_-) of the coupled motion.

The coupling coefficient C^- can be measured by approaching the tunes, e.g. by varying a single quadrupole strength (recall Eq. I.8.53) and by measuring the minimum distance between the observed tunes: $\Delta Q_{\text{min}} = |C^-|$ as shown in Fig. I.8.28.

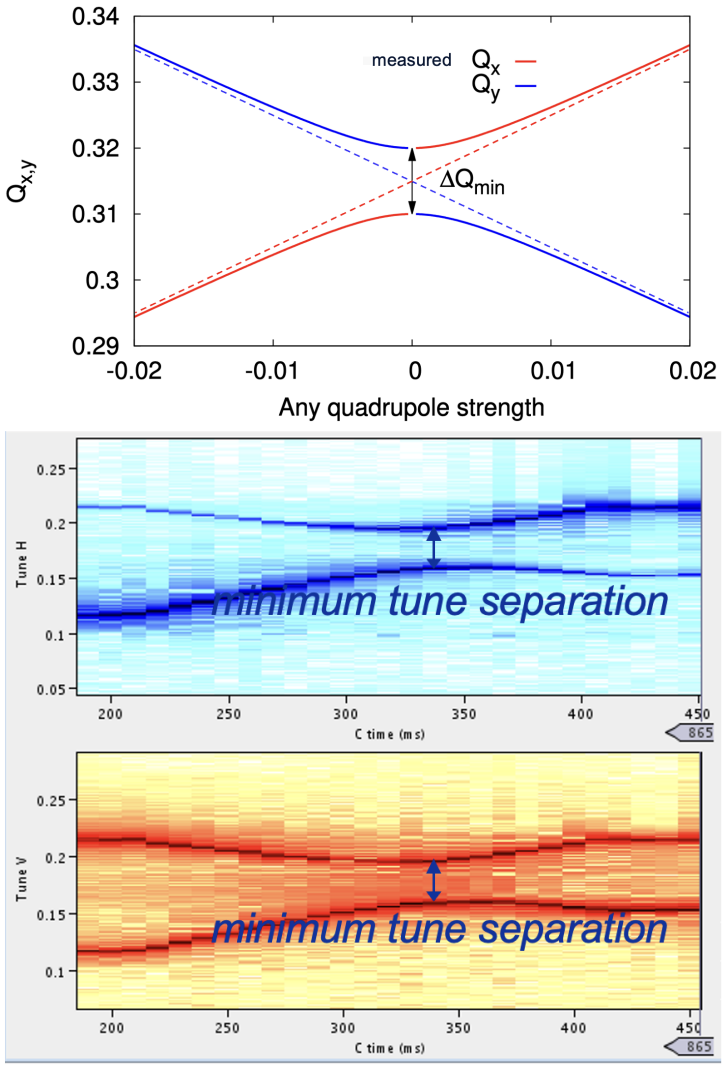

Fig. I.8.28: Conceptual experiment where coupled tunes are measured as a function of a normal quadrupole strength variation (top) and example of an actual measurement in the CERN PS (bottom). In the latter, one sees the horizontal (top) and vertical (bottom) frequency content measured on a sensitive pickup as a function of time in a cycle where the bare tunes are set to cross each other.

Coupling correctors, such as skew quadrupoles, can be introduced into the lattice to correct coupling. If skew quadrupoles are not available, vertical closed-orbit bumps in sextupole magnets can be used as a temporary measure. A typical coupling correction strategy involves:

- **Correcting the coupling coefficient:** adjust the skew-quadrupole strengths to minimize the coupling coefficient or resonance driving terms.
- **Correcting optics distortion:** correct vertical dispersion and other optics distortions induced by coupling.
- **Working point adjustment:** move the working point close to coupling resonances and iterate the correction process.

Correcting coupling is especially important for beams with unequal emittances, known as “flat

beams", for which coupling can lead to emittance exchange. Vertical orbit correction is also critical for reducing coupling, particularly due to feed-down effects in sextupoles.

I.8.4.1 Problem 7

The SPS is a 400 GeV proton synchrotron with a FODO lattice consisting of 108 focusing and 108 defocusing quadrupoles of length 3.22 m and a gradient of 15 T/m, with a horizontal and vertical beta of 108 m and 30 m in the focusing quads (30 m and 108 m for the defocusing ones). The tunes are $Q_x = 20.13$ and $Q_y = 20.18$.

In order to correct its natural chromaticity, several 0.42 m long sextupoles are installed next to focusing and defocusing quadrupoles at locations with high dispersion.

Assume that one of those sextupoles installed next to a focusing quad has a gradient of 60.3 T/m^2 and it is vertically misaligned by $\delta y = 10$ mm. Assume that the beta functions at the sextupole are equal to the ones at the nearby quadrupole.

a) What is the normalized sextupole strength?

b) Compute the impact of the vertical misalignment on:

   - tune,
   - maximum beta beating,
   - minimum tune separation,
   - maximum closed-orbit deviation

   (Neglect next order effects of such an orbit on transverse optics due to other machine sextupoles.)

c) Repeat for the case in which the sextupole is displaced horizontally.

d) What would be the maximum closed-orbit deviation if only one focusing quadrupole would be vertically displaced by $-\delta y = 10$ mm? Qualitatively, would you expect some effect on coupling or tune or beta-beating in such a case?

I.8.4.1.1 Solution to problem 7

a) – For a vertical offset in a normal sextupole, the resulting magnetic field can be computed by adapting the usual change of variable: $y \mapsto y + \delta y$:

$$B_y(x, y+\delta y) = B_2\left(x^2 - (y+\delta y)^2\right) \tag{I.8.87}$$

$$= \underbrace{B_2(x^2 - y^2)}_{\text{sextupole}} - \underbrace{2B_2(\delta y)y}_{\text{skew quad.}} - \underbrace{B_2(\delta y)^2}_{\text{dipole}}, \tag{I.8.88}$$

$$\tag{I.8.89}$$

$$B_x(x, y+\delta y) = \overbrace{B_2(2xy)} + \overbrace{2B_2(\delta y)x}\,. \tag{I.8.90}$$

  - i.e., a skew quadrupole with $\bar{A}_1 = 2B_2\delta y$ and normal dipole with $\bar{B}_0 = -B_2(\delta y)^2$ where $B_2 = 60.3\,[\text{T/m}^2]$.
  - Hence, $\bar{A}_1 = 2\times 60.3\times 0.01 = 1.21\,\text{T/m}$ and $\bar{B}_0 = -60.3\times(0.01)^2 = -0.006\,[\text{T}]$.
- With the magnetic rigidity of $B\rho = 1334\,\text{T m}$, the **normalized sextupole strength** is

$$K_2 = \frac{1}{B\rho}\frac{\partial^2 B_y}{\partial x^2} = 2\times 60.3/1334 \approx 0.09\,[\text{m}^{-3}].$$

- The skew-quadrupole normalized gradient is $\delta K_S = 1.21/1334 \approx 0.0009\,[\text{m}^{-2}]$.
- The horizontal dipole normalized field is $-0.006/1334 \approx -4.5\times 10^{-6}\,[\text{m}^{-1}]$.

b)
- Due to the skew quadrupole, we expect that minimum tune separation

$$\Delta Q_{\text{min}} \approx \frac{\sqrt{\beta_x\beta_y}}{2\pi}|\delta K_S| l_{\text{sext}} = \frac{\sqrt{108\times 30}}{2\pi}\times 0.0009\times 0.42 = 0.0034.$$

- No beta beating or tune shift is expected (a skew quadrupole does not affect beta functions).
- The kick induced by the dipole feed-down is $\theta_x = -4.5\times 10^{-6}\times 0.42 \approx 1.9\times 10^{-6}\,[\text{rad}]$.
- The maximum horizontal displacement is

$$\Delta x|_{\text{max}} = |\theta_{s_0}|\sqrt{\frac{\beta_x|_{\text{max}}\beta_x|_{s_0}}{2\sin(\pi Q_x)}} = 1.9\times 10^{-6}\sqrt{\frac{108\times 108}{2\times\sin(\pi 20.13)}} \approx 2.6\times 10^{-4}\,[\text{m}].$$

c)
- In case the offset is horizontal, one obtains a normal quadrupole and normal dipole components, hence
  - The **maximum horizontal closed orbit** would be the same as before (note that it will be on the **same plane**! as the misalignment and that the dipole kick will have a positive sign, but no change in absolute term).
  - No coupling will be introduced, as no skew components will be generated.
  - On the other hand, there will be a tune shift:

$$\delta Q_{x,y} = \pm\frac{1}{4\pi} l_{\text{sext}}\delta K\beta^F_{x,y},$$

  which correspond to:

$$\delta Q_x = \frac{0.42\times 0.0009\times 108}{4\pi} = 0.0032, \tag{I.8.91}$$

$$\delta Q_y = \frac{-0.42\times 0.0009\times 30}{4\pi} = -0.0009. \tag{I.8.92}$$

– There will also be a beta-beating

$$\left.\frac{\delta\beta_{x,y}}{\beta_{0_{x,y}}}\right|_{\text{max}} = \frac{1}{2|\sin(2\pi Q_{x,y})|}\beta^F_{x,y} l_{\text{sext}} \delta K,$$

which correspond to

$$\left.\frac{\delta\beta_x}{\beta_{0_x}}\right|_{\text{max}} = \frac{108 \times 0.42 \times 0.0009}{2|\sin(2\pi \times 20.13)|} \approx 2.8\%, \tag{I.8.93}$$

$$\left.\frac{\delta\beta_y}{\beta_{0_y}}\right|_{\text{max}} = \frac{30 \times 0.42 \times 0.0009}{2|\sin(2\pi \times 20.18)|} \approx 0.6\%. \tag{I.8.94}$$

d) – If one **focusing quadrupole** would be vertically displaced, a **vertical closed-orbit kick** would appear

$$\theta_y = \frac{G_F l_{\text{quad}}}{B\rho}\delta y = \frac{15 \times 3.22}{1334} \times 0.01 \approx 3.6 \times 10^{-4}\,[\text{rad}].$$

– The maximum vertical closed-orbit deviation (at defocusing quadrupoles) would be

$$\Delta y|_{\text{max}} = \theta_{s_0}\sqrt{\frac{\beta_y|_{\text{max}}\beta_y|_{s_0}}{2\sin(\pi Q_y)}} = 3.6 \times 10^{-4}\sqrt{\frac{108 \times 30}{2 \times \sin(\pi \times 20.18)}} \approx 20\,[\text{mm}].$$

– Such a **vertical orbit** will also be present in the sextupoles of the machine. Such a big orbit, double the misalignment considered earlier, will certainly induce **strong coupling**, but in principle no beta-beating or tune shift.

I.8.5 Summary

Linear imperfections, such as magnet misalignments and field errors, are unavoidable in a real accelerator. However, these imperfections can be corrected to some extent using various methods. The table below summarizes the main aspects of linear imperfections and their corresponding corrections.

Error source	**Effect**	**Cure**
Fabrication imperfections	Unwanted multipolar components	Better fabrication / multipolar correctors coils
Transverse misalignments	Feed-down effect	Better alignment / correctors
Dipole kicks	Orbit distortion / residual dispersion	Corrector dipoles
Quadrupole field errors	Tune shift, beta-beating	Trim special quadrupoles
Quadrupole tilts	Coupling $x - y$	Better alignment / skew quads
Power supplies	Closed-orbit distortion / tune shift / modulation	Improve power supplies and their calibration

Table I.8.1: Summary of linear imperfections and corrections in synchrotrons.

References

[1] E.D. Courant and H.S. Snyder, *Theory of the alternating-gradient synchrotron*, *Ann. Phys.* **3** (1958) 1–48, doi:10.1016/0003-4916(58)90012-5.

[2] B. Autin and Y. Marti, *Closed-orbit correction of A.G. machines using a small number of magnets*, CERN Note CERN-ISR-MA-73-17, 1973, doi:10.17181/CERN-ISR-MA-73-17.

[3] J.D. Lawrence, Transverse coupled motion, in *An introduction to the physics of high energy accelerators*, D.A. Edwards and M.J. Syphers (Wiley, Weinheim, 1993), pp. 144–171, doi:10.1002/9783527617272.ch5.

[4] I. Borchardt *et al.*, Calculation of beam envelopes in storage rings and transport systems in the presence of transverse space charge effects and coupling, *Z. Phys. C* **39** (1988) 339–349, doi:10.1007/BF01548283.

[5] D.A. Edwards and L.C. Teng, Parametrization of linear coupled motion in periodic systems, *IEEE Trans. Nucl. Sci.*, **20** (1973) 885–888, doi:10.1109/TNS.1973.4327279.

[6] E.J. Høydalsvik, T.H.B. Persson, and R. Tomas Garcia, Evaluation of the closest tune approach and its MAD-X implementation, CERN-ACC-NOTE-2021-0022 (CERN, Geneva, 2021), doi:10.17181/CERN-ACC-NOTE-2021-0022.